TsAGI

ANALYZING THE EFFECT OF SKIN POSTBUCKLING ON GENERAL STRESSES, STRAINS AND STABILITY OF COMPOSITE STRUCTURES

Prepared by:

G.N.Zamula

K.M.Ierusalimsky

G.S.Kalmykova

V.P.Fomin

1998

ABSTRACT

The present paper is a final technical report within the NCCW-1-233 research program (dated June 1, 1997) accomplished as a part of co-operation between United States' NASA and Russia's Goskomoboronprom in aeronautics, and continues similar NCCW-73 and NCC-1-233 programs accomplished in 1996 and 1997, respectively.

The report concludes studies in two domains, "Analyzing the effect of skin postbuckling on general stresses and strains in a composite structure" and "Evaluating the effect of skin postbuckling behavior on general stability of a composite structure"; the work was fulfilled in compliance with NCC-1-233 requirements (as of June 1, 1997).

Also, the present studies may be regarded as a partial generalization of efforts in [1, 2] conducted within the above programs in what concerns postbuckling behavior of composite structures.

CONTENTS

INTRODUCTION

The previous studies in [1, 2] paid major attention to postbuckling behavior of composite plates and built-up panels with consideration of nonuniform heating; the present effort deals mainly with the general strength and stability problem for a built-up structure in which some components have buckled.

In thin-walled aircraft structures the skin is known to buckle locally under loads much less than ultimate loads. So there appears the nonlinear problem to determine general stresses and load-bearing capability of the structures with buckled skins (refer to [3]). For example, static strength of a wing box in bending is usually limited by general stability of the upper stiffened panel – in which the local buckling of skin cells between stiffeners may occur at a lower load than that of the panel.

Upon skin buckling the panel is regarded as an anisotropic structure whose skin has some lowered (reduced) elastic characteristics that depend on the load level and are involved in the usual equations for computing orthotropic panel stiffnesses. Thus, two diverse problems have to be solved.

At the first stage the load should be increased gradually and the subcritical general stresses of the structure with the skin buckled should be determined by utilizing a reliable procedure (for example, with a simplified beam-based model or the finite element methods.) During these operations the element stress resultants are nonlinear functions of the load, and their values are necessary in solving the general buckling problem at each value of the (varying) load. For built-up structures (including wings and fuselages) this second problem may be solved by analytical and/or numerical methods. Let us consider main aspects of these two problems taking into account features of composite structures.

A report on the numerical method for evaluating stresses in a thin-walled structure with a buckled metal skin was delivered by the present authors in Stuttgart at the World Congress on Computational Mechanics, WCCM-II (see [3].) New reduction techniques and finite elements were used to transform the problem to classical iterations with variable elasticity parameters which are employed when calculating stresses and strains in nonlinearly elastic structures. Specific to the skin out of composites is the necessity to compute its secant reduced stiffnesses by utilizing some relatively simple relations – in particular, those derived in [1, 2]. Thus, the analytical method of [3] applies to structures with composite elements. If required, the simplified solution to the problem on postbuckling behavior of a composite plate derived in [1, 2] may also be used to estimate the strength of each buckled skin cell with consideration of in-plane forces and variable bending deformation caused by out-of-plane deflection. This problem is discussed below in Part I.

At each load value the second problem (on general instability of an isolated orthotropic panel or a cylindrical structure as a whole) may upon imposing some limitations

be solved effectively by utilizing the numerical analysis method the authors developed in [4]. However, the stability equations, unlike the stress/strain equations, are requiring the tangential stiffnesses which relate increments in generalized resultants and strains. This forces analysts to compute the tangential stiffnesses (introduced in [1]) of the buckled composite skin. Relevant issues are considered below in Part II.

In addition, both Parts pay much attention to algorithmic aspects and parametric analyses in which the features and the level of the influence of skin postbuckling on global stresses and stability of composite and metal structures. Moreover, both Parts allow for mechanical and temperature-induced loads.

It is clear that the proposed approach to allowance for the skin postbuckling effect on global stresses and stability of built-up structures is simplified and limited. However, the only real alternative thereto is a finite-element-based solution of a general geometrically nonlinear problem on very fine meshes, and this requires obtaining all local and general buckling shapes and bifurcation points for variable loads up to the structural failure loads. The latest finite-element software programs enable trying this way – but the result validity would always be in doubt.

Part I. Analyzing the effect of skin postbuckling on general stresses and strains in a composite structure

1.1 Simplified (engineering) methods for evaluating nonlinear stresses and strains in a thin-walled structure with a buckled composite skin

The influence of skin postbuckling on global stresses in a structure with a thin composite skin is very simple to consider by relying on engineering analysis methods that use a beam model suitable in dealing with long regular wing/fuselage sections.

Let us briefly outline principles of the method.

Consideration is given to a thin-walled section of a stiffened structure with a general cross-sectional shape; the global orthogonal coordinate system $0XYZ$ is introduced so that the X and Y axes are in the cross-sectional plane and the Z axis is running along the section (see Fig. 1.1.) In the cross-sectional plane the coordinate system origin is at an arbitrary point.

Both the skin thickness δ and the cross-sectional dimensions of longitudinal stiffeners are assumed to be small as compared with general cross-sectional dimensions of the structure.

For the cross section contour (at $Z = \text{const}$) we introduce the local coordinate system snz whose origin is at an arbitrary point, the s axis is tangential to the contour, the n axis is normal, and the z axis is parallel to the Z axis. The skin is made of a composite material with a symmetric layup of layer groups with various principal directions. Equivalent mechanical characteristics of the skin are determined on the basis of mechanical characteristics of orthotropic layers (E_{11}, E_{22}, G_{12}, μ_{21} and $\mu_{12} = \mu_{21} E_{22}/E_{11}$), the directions of layer groups, and volumetric fractions of the layer groups.

The equivalent mechanical characteristics E_z, E_s, $G_{zs} = G_{sz}$ and μ_{sz} correspond to the data for the orthotropic material.

The analytical method relies on the following hypotheses:

1. The cross-sectional contour (at $z = \text{const}$) is not deformable in its plane, i.e., the relative contour deformation is zero ($\varepsilon_s = 0$).

2. Strain in any cross section is described by the plane equation:

$$\varepsilon_z = \varepsilon_o + \theta'_y x + \theta'_x y \quad , \tag{1.1}$$

Herein, ε_o, θ'_y and θ'_x are certain functions of z; the prime sign designates differentiation with respect to z.

Now we use conventional stress/strain relations for an orthotropic skin

$$\varepsilon_z = \frac{\sigma_z}{E_z} - \mu_{sz}\frac{\sigma_s}{E_s}, \qquad \varepsilon_s = \frac{\sigma_s}{E_s} - \mu_{zs}\frac{\sigma_z}{E_z} = 0,$$

to derive the normal stress σ_z profile over the sectional contour:

$$\sigma_z = \frac{E_z}{1 - \mu_{sz}\mu_{zs}}\left(\varepsilon_o + \theta'_y x + \theta'_x y\right) \tag{1.2}$$

As usual, $\sigma_s = -\mu_{sz}\sigma_z$.

3. Since the skin thickness δ is thin, the skin is assumed not to take bending, so its tangential stress τ and normal stress σ_z are distributed uniformly throughout the thickness direction. In this case it is convenient to introduce the normal stress resultant and the tangential stress flow by using, respectively,

$$N_o = \sigma_z \delta, \quad q = \tau\delta. \tag{1.3}$$

The flow q is tangential to the cross section contour. Similarly, stiffener sizes are small in relation to the cross section contour sizes; therefore, we are allowed to assume that the stiffener cross-sectional area f_s is concentrated at the relevant contour point and that its force is $P_s = f_s\sigma_{zs}$ where σ_{zs} is the stiffener stress.

4. At each cross section $z = \text{const}$ external loads are

- bending moments $M_x(z)$, $M_y(z)$,
- torsional moment $M_z(z)$,
- axial force $N_z(z)$,
- shear forces $Q_x(z)$ and $Q_y(z)$,

these are referred to the axes X, Y, and Z above. Positive directions for the external factors may be seen in Fig. 1.1.

Note that these factors satisfy the relations,

$$\frac{dM_x}{dz} = Q_y, \quad \frac{dM_y}{dz} = -Q_x \tag{1.4}$$

Evaluating the normal stresses

Unknown values of ε_o, θ'_y and θ'_x should be determined from equilibrium equations:

$$\begin{aligned}
&\oint \sigma_z \delta ds + \sum_{i=1}^{n} \sigma_{zsi} f_{si} = N_z; \\
&\oint \sigma_z y ds + \sum_{i=1}^{n} \sigma_{zsi} f_{si} y_i = M_x; \\
&\oint \sigma_z x ds + \sum_{i=1}^{n} \sigma_{zsi} f_{si} x_i = -M_y,
\end{aligned} \tag{1.5}$$

Here, σ_z is the skin stress,

σ_{zsi} is the stress in an i-th stiffener,

δ is the skin thickness,

f_{si} is the cross-sectional area of the i-th stiffener, and

n is the total number of stiffeners in the section.

If stiffeners are rather numerous, the integrals can be estimated in a simple way by adding to each stiffener a half of the areas of the skin cells neighbouring with the stiffener (see Fig. 1.1.) In this case the integrals in (1.5) become finite sums; using (1.2) we have

$$\begin{aligned} E\sum_{i=1}^{n} F_{si}\varepsilon_{zi} &= N_z, \\ E\sum_{i=1}^{n} F_{si}y_i\varepsilon_{zi} &= M_y, \\ E\sum_{i=1}^{n} F_{si}x_i\varepsilon_{zi} &= -M_y, \end{aligned} \tag{1.6}$$

where

$$F_{si} = r_{si}f_{si} + \frac{1}{2}\sum_{j\in\omega(i)} r_{oj}\varphi_j^s\delta_j b_{sj}\,, \tag{1.7}$$

Summation in (1.7) is for the set $\{\omega(i)\}$ of panels neighbouring with the i-th node,

$$r_{si} = E_{si}/E, \quad r_{oj} = \frac{E_{zj}}{\left(1-\mu_{szj}^s\mu_{zsj}^s\right)E},$$

E is the Young's modulus of the material to which the characteristics of stiffeners and skin cells are reduced,

E_{zj} is the Young's modulus of a j-th cell, $E_{zj}^s = \varphi_j^s E_{zj}$,

φ_j^s is the secant reduction coefficient for the j-th cell (with $\varphi_j^s < 1$ if the cell buckles),

μ_{szj}^s and μ_{zsj}^s are secant Poisson's ratios for the j-th cell upon buckling, and

b_{sj} is the width of the j-th cell.

Formulas for computing μ_{szj}^s, μ_{zsj}^s and φ_j^s are presented in [1].

As (1.1) postulates, $\varepsilon_{zi} = \varepsilon_o + \theta'_y x_i + \theta'_x y_i$, so we can re-write (1.6) as,

$$E\cdot\begin{vmatrix} F & S_x & S_y \\ S_x & I_x & I_{xy} \\ S_y & I_{xy} & I_y \end{vmatrix}\begin{Bmatrix} \varepsilon_o \\ \theta'_x \\ \theta'_y \end{Bmatrix} = \begin{Bmatrix} N_z \\ M_x \\ -M_y \end{Bmatrix}, \tag{1.8}$$

Here, $F = \sum_{i=1}^{n} F_{si}$ is the generalized cross section area,

$S_x = \sum_{i=1}^{n} F_{si}y_i$ is the generalized area moment for the x axis,

$S_y = \sum_{i=1}^{n} F_{si}x_i$ is the generalized area moment for the y axis,

$I_x = \sum_{i=1}^{n} F_{si}y_i^2$ is the generalized moment of inertia for the x axis,

$I_y = \sum_{i=1}^{n} F_{si}x_i^2$ is the generalized moment of inertia for the y axis, and

$I_{xy} = I_{yx} = \sum_{i=1}^{n} F_{si}x_i y_i$ is the generalized product of inertia.

The system (1.8) is nonlinear because the generalized sectional characteristics include the reduction factors φ_j^s which depend on skin stresses (upon buckling) — and on unknown values of ε_o, θ'_x and θ'_y.

Therefore, the normal stress in structural components should be determined by iterations with external loads being increased in increments. At a fixed external load (the vector $\{N_z, M_x, M_y\}$) the analysis runs as follows.

Initially, all reduction factors φ_j^s are set to 1. Equation (1.7) is used to compute F_{si} for all values of i and establish the matrix with generalized sectional characteristics. The system (1.8) is solved to evaluate ε_o, θ'_x and θ'_y. The formula (1.2) provides stresses in skin cells. If these stresses are greater than critical for at least one panel, the respective secant reduction factors φ_j^s and secant Poisson's ratios are calculated by employing relations from [1]. The reduction factors and Poisson's ratio values are used to obtain F_{si} from (1.7) and the matrix of generalized sectional characteristics. The system (1.8) is solved to again evaluate ε_o, θ'_x and, θ'_y. The successive iteration process does usually converge for 3 or 4 cycles.

Determining shear stresses

To determine the skin shear stress flow q we should consider the equilibrium condition for a skin element ds dz (Fig. 1.2) at N_z = const:

$$\frac{\partial \sigma_z}{\partial z}\delta + \frac{\partial q}{\partial s} = 0 \ . \tag{1.9}$$

Then the shear stress flow may be written as,

$$q = q_Q + q_o(z), \tag{1.10}$$

where $q_Q = -\int_0^s \frac{\partial \sigma_z}{\partial z}\delta\, ds$ and q_o is an unknown closing flow.

Now we employ the above discrete section model to write:

$$q_{Qi} = -\sum_{i=1}^{i}\frac{\partial \sigma_{zi}}{\partial z}\delta_i s_i = -E\sum_{i=1}^{i}F_{si}\frac{\partial}{\partial z}\left(\varepsilon_o + \theta'_y x_i + \theta'_x y_i\right) = = -E\sum_{i=1}^{i}F_{si}\left(\varepsilon'_o + \theta'_y x_i + \theta'_x y_i\right). \tag{1.11}$$

Differentiate equations (1.8) with respect to z and involve (1.4) to obtain,

$$E\cdot\begin{vmatrix} F & S_x & S_y \\ S_x & I_x & I_{xy} \\ S_y & I_{xy} & I_y \end{vmatrix}\begin{Bmatrix} \varepsilon'_o \\ \theta''_x \\ \theta''_y \end{Bmatrix} = \begin{Bmatrix} 0 \\ Q_y \\ Q_x \end{Bmatrix}. \tag{1.12}$$

Thus, for us to determine the derivatives ε'_o, θ''_y and θ''_x (present in (1.11)) we have equation (1.12) in which the matrix of generalized sectional characteristics is the same as

that in (1.8), and the right-hand side vector contains shear forces. With this set of equations solved, the shear stress flow is calculated by (1.11) taking into consideration that

$$\tilde{F}_i = \sum_{i=1}^{i} F_{si}\,, \quad \tilde{S}_{xi} = \sum_{i=1}^{i} F_{si}\, y_i\,, \quad \tilde{S}_{yi} = \sum_{i=1}^{i} F_{si}\, x_i \quad - \tag{1.13}$$

are the generalized sectional area and the static moments of the cut part; these are computed allowing for sectional topology. The closing flow q_o is established by satisfying the equilibrium equation for the torsional moment M_z.

If the sectional contour is simply connected, the flow q_o is described by the Bredt formula:

$$q_o = \frac{M_z}{\Omega}\,, \tag{1.14}$$

in which the symbol Ω denotes the doubled internal area.

If, however, the section is multiply connected, the closing flows q_{oj} should be estimated by involving both the equilibrium equation and strain compatibility relations for edges of the contours; taken together, these provide the number of equations necessary for us to determine all flows q_{oj}.

In case the skin cells buckle under compression/shear, this circumstance is allowed for when estimating the reduction factors φ_j^s by the method explained in [1]. Problems on normal stresses and shear flow are solved jointly at each iteration for determining reduction factors φ_j^s and Poisson's ratios μ_{zsj}^s and μ_{szj}^s with consideration of shear stress.

This approach has been implemented in the composite structure section behavior analysis software.

These means were utilized to investigate into the influence of postbuckling skin deformation on global stresses in a stiffened cylindrical structure. Two examples were treated in order to evaluate in numbers the significance of these factors in stress analyses.

The first example is a circular cylinder with a 2540-mm diameter, loaded with a bending moment and a torsional moment, see Fig. 1.3. Distances b_s between longitudinal stiffeners are identical throughout the contour, and the frame spacing ℓ_f is 500 mm. The skin is a 2.64-mm thick composite stack comprising 22 layers whose stacking sequence is $\left[0_5/90_2/45_2/-45_2\right]_s$. Equivalent skin data computed for the particular volume fractions and ply angles are as follows: $E_z = 6682\,\text{kg/sq.mm}$, $E_s = 3768\,\text{kg/sq.mm}$, $G_{zs} = 1434\,\text{kg/sq.mm}$, μ_{zs}=0.3187. Similarly, skin ultimate stresses are $\sigma_{fz}^c = 44.5\,\text{kg/sq.mm}$ in compression, $\sigma_{fz}^t = 31.2\,\text{kg/sq.mm}$ in tension, and $\tau_{fzs} = 24.8\,\text{kg/sq.mm}$ in shear.

Consideration is given to two versions of longitudinal stiffening (see Fig. 1.4); these differ in the stiffener spacing ($b_{s1} = 100\,\text{mm}$ and $b_{s2} = 125\,\text{mm}$) and the stiffener section area ($f_{s1} = 200\,\text{sq.mm}$ and $f_{s2} = 247\,\text{sq.mm}$). The sectional areas, f_{s1} and и f_{s2}, are chosen such that the total stiffener areas for the two versions are equal. With this, the equivalent stiffener data are as follows: $E_z = 8346\,\text{kg/sq.mm}$, ultimate compressive stress $\sigma^c_{fz} = 55.5\,\text{kg/sq.mm}$, and ultimate tensile stress $\sigma^t_{fz} = 39.0\,\text{kg/sq.mm}$. The structures are analyzed while proportionally increasing the external load vector:

$$M_x = t\,M_{xo}\,, \quad M_x = t\,M_{xo}\,,$$

(where t is the increasing proportionality coefficient) for two load patterns:

a) pure bending with $M_{xo} = 5\cdot 10^6\ \text{kg}\cdot\text{mm}$ and $M_{zo} = 0$,

b) bending and torsion with $M_{xo} = 5\cdot 10^6\ \text{kg}\cdot\text{mm}$ and $M_{zo} = 2.55\cdot 10^6\ \text{kg}\cdot\text{mm}$.

Calculated stresses for these stiffening schemes and load conditions are shown in Figs 1.5 and 1.6 representing the lower stiffener stresses and mean stresses in the lowest (compressed) skin cell; the argument here is the load parameter $t = M_x/M_{xo}$. Figure 1.5 is to the load condition a); and Fig. 1.6, to the load condition b). Let us first discuss the results for the structure loaded in bending (Fig. 1.5.)

Two straight lines (rays) which are running through the coordinate system origin and marked with circles demonstrate the linear analysis not allowing for skin reduction at the postbuckling stage. The upper ray reflects stiffener stresses, and the lower one, the skin stress. Solid fine lines represent stiffener stresses and the mean skin stress in case the skin reduction upon buckling is carried out. One can see that in the structure with the spacing $b_{s1} = 100\,\text{mm}$ the lower cell buckles at $t \approx 0.58$. With the load growing, the stiffener stresses increase, whereas mean skin stresses fall in comparison with linear analysis results. In the structure with the spacing $b_{s2} = 125\,\text{mm}$ the skin gets buckled at an earlier time: $t \approx 0.38$; in other respects the stiffener stresses and mean skin stresses behave like those characteristics of the former version. It should be mentioned that stresses notably re-distribute in comparison with the linear analysis and the difference increases as the postbuckling level gets higher.

Moreover, the skin reduction amount varies in the vertical direction, so the neutral axis is shifted to tension-loaded panels and this circumstance, in turn, causes the compression-loaded structural part to take a greater force. Thus, the compression-loaded stiffeners are carrying additional forces because of not only the "early" skin buckling but also the neutral axis shift.

The results for the case with bending and torsion are depicted in Fig. 1.5. These are similar to those in Fig. 1.6. Note that skin buckling stresses σ_z have diminished since the skin is made to also carry in-plane shear. In this case the lower panel features the ratio $\tau/\sigma_z = 0.5$

When assessing strength of a buckled skin cell, we must compute the total maximum stresses through the thickness which are comprising the middle-surface stress and the bending stress depending on local skin displacement $w(x, y)$. These stresses may be computed by the method exposed in [1].

Figure 1.7 depicts the dependence of the lower skin maximum stress (referred to the ultimate stress $\bar{\sigma}$) on the parameter $t = M_x/M_{xo}$ for the case a). The total stress σ_z at the point $\{s/b_s = 0.5,\ z = \ell_x/2,\ h = \delta/2\}$ reach the breaking condition

– at $M_x/M_{xo} \approx 0.92$ for the cell with $b_{s1} = 100\,\text{mm}$ and

– at $M_x/M_{xo} \approx 0.98$ for the cell with $b_{s2} = 125\,\text{mm}$.

Figure 1.8 shows a similar kind of dependence for the load case b). Torsion decreases the value of $t = M_x/M_{xo}$ at which the breaking stress is attained:

– $M_x/M_{xo} \approx 0.76$ for $b_{s2} = 125\,\text{mm}$ and - $M_x/M_{xo} \approx 0.82$ for $b_{s1} = 100\,\text{mm}$.

Coordinates of the point with the hardest load depend on the external load. As for the above value of M_x/M_{xo}, the breaking stress is attained at the point with coordinates $s/b_s \approx 0.3$; $z \approx 0.3\ell_x$.

The second example is a rectangular cylinder with the 2000-mm width and the 1000-mm height, loaded with bending or bending+torsion, see Fig. 1.9. The rib spacing ℓ_f equals 500 mm. Upper and lower panels and vertical side walls are 4.56-mm thick composite materials with 38 layers stacked as $[0_{10}/90_3/45_3/-45_3]_s$. Equivalent skin data are as follows: E_z=7383 kg/sq.mm, E_s=3407 kg/sq.mm, G_{zs}=1311 kg/sq.mm, μ_{zs}=0.3217. Skin ultimate stresses are $\sigma^c_{fz} = 49.2\,\text{kg/sq.mm}$ in compression, $\sigma^t_{fz} = 34{,}5\,\text{kg/sq.mm}$ in tension, and $\tau_{fzs} = 26.7\,\text{kg/sq.mm}$ in shear.

Consideration is given to two versions of longitudinal stiffening, see Fig. 1.10; these differ in the stiffener spacing ($b_{s1} = 125\,\text{mm}$ and $b_{s2} = 167\,\text{mm}$) and the stiffener section area ($f_{s1} = 247\,\text{sq.mm}$ and $f_{s2} = 323\,\text{sq.mm}$). The sectional areas are specified so that the total stiffener areas for both versions are equal. Equivalent stiffener data are the same as for the first example.

Structures are analyzed for two load patterns:

a) pure bending (with the upper panel being in compression and the lower panel subjected to tension) and

b) bending + torsion

while proportionally increasing the external load vector for $M_{xo} = 3\cdot10^6\,\text{kg}\cdot\text{mm}$ and $M_{zo} = 1.97\cdot10^6\,\text{kg}\cdot\text{mm}$.

Stresses calculated with and without allowance for nonlinearity are shown in Figs 1.11 and 1.12; as in the case with the circular cylinder the skin and stiffener stresses are functions of the load parameter t. Figure 1.11 is for the pure bending, and Fig. 1.12, for bending + torsion. Figures 1.13 and 1.14 represent how the maximum stress in the compressed skin varies with t; here, the "circle" ($\circ$) sign denotes values $\sigma_z/\overline{\sigma} = 1$ that correspond to loads under which the stress at the external skin surface become equal to the ultimate values.

Qualitatively, the postbuckling deformation of the skin influences global stresses and strains in the same manner as in the circular structure. Note that the wing skin is usually thicker than the fuselage skin and is allowed to buckle under loads that exceed the in-service values. Therefore, the skin reduction influence on global stress/strain fields in the wing is less pronounced than that in the fuselage. In addition, wing skin reduction does not almost result in additional load for compression-loaded panels – because spar webs give a little contribution to the wing bending stiffness, and the forces taken by upper and lower panels are mainly defined by the bending moment and the section height. In the example above, the typical wing situation is modeled by the structure with $b_{sl} = 125\text{mm}$ and $f_{sl} = 247\text{sq. mm}$, and the skin buckles at $t \approx 0.93$.

1.2. Nonlinear finite-element methods taking into account skin postbuckling behavior

An overall algorithm for numerically analyzing strength and stability of a thin-walled structure with a buckled skin is depicted in Fig. 1.15. Here, t stands for any increasing parameter (it may be time) which is an argument for loads; $0 < \varphi^s \le 1$ and $0 < \varphi^t \le 1$ are secant and tangential reduction factors that evaluate degradation of elastic characteristics of the locally buckled skin; t_* is the value of the parameter at which the structure fails because of

a) general buckling or

b) destruction of primary components not buckled or

c) destruction of the buckled (composite or metallic) skin.

In the latter case we must pay attention not only to strength criteria with in-service loads but also to

- requirements on allowable skin displacements and
- the criterion of not reaching the yield strain (for metals) or of first-ply failure (for composites) under in-service loads.

The problem is nonlinear because the skin reduction factors depend on skin stresses; note that, according to [1, 2], the buckled skin is modeled by a stiffness-equivalent non-buckled orthotropic plate made out of a nonlinearly elastic material.

When analyzing global stresses of thin-walled structures by means of finite-element programs, the stiffened panels and walls are usually modeled with triangular and quadrilateral orthotropic plane-stress finite elements (Fig. 1.16a); nonlinearity is dealt with at each value of t by conducting additional iterations which refine φ^s. Stiffeners surrounding a skin cell are usually spaced rather closely and deform in compatibility with it; therefore, the problem is below proposed to be solved by using new types of built-up finite elements comprising the skin and stiffeners; these are convenient in allowing for postbuckling behavior. In this case the composite skin orthotropy axes are assumed to coincide with stiffener directions; the skin and stiffeners may have different temperatures.

Finite-elements

Consider a thin-gage triangular or quadrilateral plate of thickness δ orthogonally stiffened with ribs (in x - and y directions, at spacing ℓ_1, ℓ_2 and cross-sectional areas F_1, F_2). A skin material is assumed to be orthotropic, with principal axes running along the stiffeners. Local coordinate systems have x_m, y_m and x'_m, y'_m planes in a middle surface of the skin (Fig. 1.16b), the structure is located in a global coordinate system 0xyz as desired. A skin temperature field is considered uniform, of value T_{sk}, whereas a stiffener temperature varies along the z - axis, the same law being assumed for all stiffeners of the same direction. To transform this model to an orthotropic material membrane, use can be made of the «orthotropic layer» concept (by Birger, Ref. 5) with «core coefficients» K_x, K_y and K_γ for x'_m and y'_m — directions and for shear, respectively. Then, the elasticity relations for the layer may be written as

$$\varepsilon_x=\frac{\sigma_x}{E_x}-\frac{\nu_y K_y \sigma_y}{E_y}+\Delta_x,\quad \varepsilon_y=\frac{\sigma_y}{E_y}-\frac{\nu_x K_x \sigma_x}{E_x}+\Delta_y,\quad \gamma_{xy}=\frac{\tau_{xy}K_x}{GK_\gamma}=\frac{\tau_{yx}K_y}{GK_\gamma} \tag{1.15}$$

or, in terms of stresses,

$$\begin{aligned}
\sigma_x &= \frac{E_x}{1-\nu_x\nu_y K_x K_y}(\varepsilon_x-\Delta_x)+\frac{\nu_y K_y E_x}{1-\nu_x\nu_y K_x K_y}(\varepsilon_y-\Delta_y),\\
\sigma_y &= \frac{E_y}{1-\nu_x\nu_y K_x K_y}(\varepsilon_y-\Delta_y)+\frac{\nu_x K_x E_y}{1-\nu_x\nu_y K_x K_y}(\varepsilon_x-\Delta_x),\\
\tau_{xy} &= \frac{GK_\gamma}{K_x}\gamma_{xy},\quad \tau_{yx}=\frac{GK_\gamma}{K_y}\gamma_{xy},\quad (\nu_y=\mu_{xy},\nu_x=\mu_{xy}).
\end{aligned} \tag{1.16}$$

Here, $\Delta_x=\alpha_x(T-T_o)$, $\Delta_y=\alpha_y(T-T_o)$ are the thermal expansions, T_o is the initial temperature of panel. Integrating over periodical structural elements (Fig. 1.16c) and assuming the in-plane deformation, one can derive the following elasticity relations:

$$N_x = f_{1x}(\varepsilon_x - \varepsilon_{xo}) + f_2(\varepsilon_y - \varepsilon_{yo}),$$
$$N_y = f_2(\varepsilon_x - \varepsilon_{xo}) + f_{1y}(\varepsilon_y - \varepsilon_{yo}), \qquad (1.17)$$
$$N_{xy} = N_{yx} = f_{1\gamma}\gamma_{xy},$$

where

$$f_{1x} = \int_{-\delta/2}^{h-\delta/2} \frac{E_x K_x}{1-\nu_x\nu_y K_x K_y} dz_m, \quad f_{1y} = \int_{-\delta/2}^{h-\delta/2} \frac{E_y K_y}{1-\nu_x\nu_y K_x K_y} dz_m,$$
$$f_2 = \int_{-\delta/2}^{h-\delta/2} \frac{E_x \nu_y K_x K_y}{1-\nu_x\nu_y K_x K_y} dz_m, \quad f_{1\gamma} = \int_{-\delta/2}^{h-\delta/2} G K_\gamma dz_m \qquad (1.18)$$

are stiffnesses of the panel,

$$\varepsilon_{xo} = \frac{f_{1y}T_{1x} - f_2 T_{1y}}{f_{1x}f_{1y} - f_2^2}, \quad \varepsilon_{yo} = \frac{f_{1x}T_{1y} - f_2 T_{1x}}{f_{1x}f_{1y} - f_2^2},$$
$$T_{1x} = \int_{-\delta/2}^{h-\delta/2} \frac{E_x K_x(\Delta_x + \nu_y K_y \Delta_y)}{1-\nu_x\nu_y K_x K_y} dz_m, \quad T_{1y} = \int_{-\delta/2}^{h-\delta/2} \frac{E_y K_y(\Delta_y + \nu_x K_x \Delta_x)}{1-\nu_x\nu_y K_x K_y} dz_m \qquad (1.19)$$

are temperature strains and stress resultants.

Eqs (1.15) to (1.19) are the same as formulae of Ref. 4, if the material used is isotropic, but they are convenient for FEM codes to use. Really, eqs (1.17) correspond to the typical matrix formulation:

$$\{N\} = [D]\big(\{\varepsilon\} - \{\varepsilon_o\}\big), \qquad (1.20)$$

where

$$[D] = \begin{bmatrix} f_{1x} & f_2 & 0 \\ f_2 & f_{1y} & 0 \\ 0 & 0 & f_{1\gamma} \end{bmatrix}$$

is the constitutive matrix, $\{N\} = [N_x\ N_y\ N_{xy}]^T$, $\{\varepsilon\} = [\varepsilon_x\ \varepsilon_y\ \gamma_{xy}]^T$, $\{\varepsilon_o\} = [\varepsilon_{xo}\ \varepsilon_{yo}\ 0]^T$ are vectors of stress resultants, and initial strains, respectively. After dividing eq (1.20) by the skin thickness δ and after comparing (1.20) to (1.16) at $K_x = K_y = K_\gamma = 1$, one can see that, in place of the panel, there is a membrane of thickness δ, temperature T_{sk}, average stresses $\{\sigma\} = [\sigma_x\ \sigma_y\ \tau_{xy}]^T = 1/\delta\{N\}$, made of an orthotropic material whose characteristics is principal directions $(x'_m,\ y'_m)$ are $\bar{E}_x$, $\bar{E}_y$, $\bar{G}$, $\bar{\nu}_y$, $\bar{\alpha}_x$, $\bar{\alpha}_y$, so that

$$\{\bar{\sigma}\} = [\bar{D}]\big(\{\varepsilon\} - \{\varepsilon_o\}\big), \quad [\bar{D}] = \frac{1}{\delta}[D] = \begin{bmatrix} \dfrac{\bar{E}_x}{1-\bar{\nu}_x\bar{\nu}_y} & \dfrac{\bar{E}_x\bar{\nu}_y}{1-\bar{\nu}_x\bar{\nu}_y} & 0 \\ \dfrac{\bar{E}_y\bar{\nu}_x}{1-\bar{\nu}_x\bar{\nu}_y} & \dfrac{\bar{E}_y}{1-\bar{\nu}_x\bar{\nu}_y} & 0 \\ 0 & 0 & \bar{G} \end{bmatrix}, \qquad (1.21)$$

where $\{\varepsilon_o\} = \big[\bar{\alpha}_x(T_{o6} - T_o)\ \bar{\alpha}_y(T_{o6} - T_o)\ 0\big]^T$ and

$$\bar{E}_x = \frac{\bar{f}_{1x}\bar{f}_{1y} - \bar{f}_2^2}{\bar{f}_{1y}},\ \bar{E}_y = \frac{\bar{f}_{1x}\bar{f}_{1y} - \bar{f}_2^2}{\bar{f}_{1x}},\ G = \bar{f}_{1\gamma},\ \bar{\nu}_y = \frac{f_2}{f_{1x}},\ \bar{\nu}_x = \frac{f_2}{f_{1y}} = \bar{\nu}_y \frac{\bar{E}_x}{\bar{E}_y},$$
$$\bar{\alpha}_x = \frac{\varepsilon_{xo}}{T_{об} - T_o},\ \bar{\alpha}_y = \frac{\varepsilon_{yo}}{T_{об} - T_o},\ \bar{f}_{1x} = \frac{f_{1x}}{\delta},\ \bar{f}_{1y} = \frac{f_{1y}}{\delta},\ \bar{f}_2 = \frac{f_2}{\delta}, \bar{f}_{1\gamma} = \frac{f_{1\gamma}}{\delta}. \quad (1.22)$$

After integration in (1.18) and (1.19), formulae (1.22) can be used for specifying material properties in usual structural analyses with triangular and/or quadrilateral membrane FEs. However, it is important to note that the actual stress field is represented by eqs (1.16) instead of (1.21). In particular, a skin experiences, as rule, additional local stress due to restraint from stiffeners of lower temperature; this circumstance become important while analyzing whether the skin can buckle (and at reducing the skin, if any). Hereinafter, let's use a simplifying assumption of a small values of $K_\gamma << 1$, and $\nu_y K_y << 1$, $\nu_x K_x << 1$ for all parts of the panel under study. Such an assumption is usually valid for typical airframes. Then, the skin is characterized by $K_x = K_y = K_\gamma = 1$. Eqs (1.18) will be transformed:

$$f_{1x} = \frac{E_x\delta}{1-\nu_x\nu_y} + \frac{\bar{E}_1 F_1}{\ell_1},\quad f_{1y} = \frac{E_y\delta}{1-\nu_x\nu_y} + \frac{\bar{E}_2 F_2}{\ell_2},\quad f_2 = \frac{E_x\nu_y\delta}{1-\nu_x\nu_y},\quad f_{1\gamma} = G\delta, \quad (1.23)$$

where E_x, E_y, G, ν_y are the elastic constants of skin at temperature T_{sk},

$$\bar{E}_1 = \frac{1}{F_1}\int_{F_1} E_1\, dF,\quad \bar{E}_2 = \frac{1}{F_2}\int_{F_2} E_2\, dF$$

are the averaged moduli of stiffeners. By parity of reasoning with eq. (1.19), obtain

$$T_{1x} = \frac{E_x\delta}{1-\nu_x\nu_y}(\alpha_x + \nu_y\alpha_y)(T_{об} - T_o) + \frac{\bar{E}_1 F_1}{\ell_1}\bar{\Delta}_1,\quad \bar{\Delta}_1 = \frac{1}{\bar{E}_1 F_1}\int_{F_1} E_1\alpha_1(T_1 - T_o)\,dF,$$
$$T_{1y} = \frac{E_y\delta}{1-\nu_x\nu_y}(\alpha_y + \nu_x\alpha_x)(T_{об} - T_o) + \frac{\bar{E}_2 F_2}{\ell_2}\bar{\Delta}_2,\quad \bar{\Delta}_2 = \frac{1}{\bar{E}_2 F_2}\int_{F_2} E_2\alpha_2(T_2 - T_o)\,dF, \quad (1.24)$$

where $\bar{\Delta}_1$ and $\bar{\Delta}_2$ are the averaged thermal elongations of stiffeners. Eqs (1.16) give stresses

$$\sigma_x = \frac{E_x(1-\nu_y\bar{\nu}_x)}{\bar{E}_x(1-\nu_x\nu_y)}\bar{\sigma}_x + \frac{E_x(\nu_y - \bar{\nu}_y)}{\bar{E}_y(1-\nu_x\nu_y)}\bar{\sigma}_y - \frac{E_x}{1-\nu_x\nu_y}\left[(\alpha_x + \nu_y\alpha_y)(T_{об} - T_o) - \varepsilon_{xo} - \nu_y\varepsilon_{yo}\right],$$
$$\sigma_y = \frac{E_y(1-\nu_x\bar{\nu}_y)}{\bar{E}_y(1-\nu_x\nu_y)}\bar{\sigma}_y + \frac{E_y(\nu_x - \bar{\nu}_x)}{\bar{E}_x(1-\nu_x\nu_y)}\bar{\sigma}_x - \frac{E_y}{1-\nu_x\nu_y}\left[(\alpha_y + \nu_x\alpha_x)(T_{об} - T_o) - \varepsilon_{yo} - \nu_x\varepsilon_{xo}\right], \quad (1.25)$$
$$\tau_{xy} = \frac{G}{\bar{G}}\bar{\tau}_{xy} = \tau_{xy}$$

for a skin,

$$\sigma_x = \frac{E_1}{\bar{E}_x}\bar{\sigma}_x - \frac{E_1\bar{\nu}_y}{\bar{E}_y}\bar{\sigma}_y - E_1\left[\alpha_1(T_1 - T_o) - \varepsilon_{xo}\right],\quad \tau_{xy} = 0,$$
$$\sigma_y = \frac{E_2}{\bar{E}_y}\bar{\sigma}_y - \frac{E_2\bar{\nu}_x}{\bar{E}_x}\bar{\sigma}_x - E_2\left[\alpha_2(T_2 - T_o) - \varepsilon_{yo}\right],\quad \tau_{yx} = 0 \quad (1.26)$$

for stiffeners.

It can be seen from (1.23)-(1.26) that both determination of skin stresses and reduction of skin require only a few data: skin parameters and integral characteristics of stiffeners, namely, F_1, ℓ_1, E_1, Δ_1, F_2, ℓ_2, E_2, Δ_2.

To perform a strength analysis of such finite elements, one should apply usual relations of the Finite Element Method, Ref. 5; in addition, an elastic and thermal performance of the skin and the stiffeners can be specified. Hereinafter, the parameters involved are assumed to be the same over all skin and over all stiffeners of the same direction.

A triangular stiffened panel (Fig. 1.16b) carries in-plane axial loads and shear. The displacement field in the element is assumed to be linear. For the plane-stress element with a uniform thickness δ the stiffness matrix is,

$$[K] = \delta \int_A [B]^T [\tilde{D}][B] dA, \tag{1.27}$$

Here,

$[\tilde{D}]$ is the matrix with reduced element stiffnesses referred to the local $\{x_m, y_m\}$ coordinate system and derived from $[\overline{D}]$ (see (1.21)) by transforming the coordinates;

$[B]$ is the usual constant matrix for computing the strains $\{\varepsilon\} = [B]\{q\}$.

Upon integrating the relation (1.27) the explicit formulas for the element stiffnesses referred to the local coordinate system appear.

Equilibrium equations taking into account initial thermal strains are,

$$[K]\{q\} = \{F\} + \{F\}_{\varepsilon_o}$$

Here,

$\{F\}$ is the nodal force vector due to the external loads and

$\{F\}_{\varepsilon_o}$ is the initial thermal force vector which may be evaluated as

$$\{F\}_{\varepsilon_o} = \delta \int_A [B]^T [\tilde{D}]\{\varepsilon_o\} dA$$

The FEM problem is then solved to determine nodal displacements $\{q\}$, strains $\{\varepsilon\}$; thereafter, (1.21) is utilized to calculate average stresses, and relations (1.25) and (1.26) are used to compute the stress field for the panel.

A quadrilateral stiffened panel (Fig. 1.16b) is to be modelled by a simple finite element whose thickness is that of skin, and thermo-mechanical characteristics (1.23), (1.24) take account of performance of both skin and stringers. A stiffness matrix can be derived as suggested in Ref. [6]. That is, the quadrilateral structure should be separated into four triangles, and displacements of the additional internal node should be eliminated. Each triangle has a linear displacement field and a uniform stress state. For each triangle, a structural analysis system can compute a stiffness matrix, strains, and stresses by means of the above formulae.

Unfortunately, such FEs produce significant errors if used in areas of severe stress gradients, say, in models of spar walls subjected to bending.

An accuracy can be improved through introducing the quadratic incompatible shape functions, their coefficients being found under conditions of minimum strain energy of the finite element, Ref 7. A new FE — quadrilateral stiffened wall — has been a good complement for the existing FEs of our structural analysis system. It represents a futher improvement of the FE proposed in Ref. 7 and allows for additional internal structures, orthotropic material, and temperature gradients. The stiffness matrix components can be computed using the Gauss-Legendre four-point integration formulae, Ref: 6; eq. (1.21) is a source of the matrix of elastic constants. The finite elements proposed can be developed further to include different structural features.

Solving the nonlinear problem

As stated above, consideration of plastic deformation and buckling of the skin makes us regard stiffnesses of the skin (and the panel as a whole) as functions of an instantaneous level of stresses and strains:

$$[\overline{D}] = [\overline{D}(\{\varepsilon\},\{\sigma\})], \quad \{\varepsilon_o\} = \{\varepsilon_o(\{\varepsilon\},\{\sigma\})\}, \tag{1.28}$$

where $\{\sigma\} = [\sigma_x \sigma_y \tau_{xy}]^T$ is the skin stress vector in accordance with (1.25).

The nonlinear problem may be solved on the basis of the FEM and the proposed finite elements by resorting to iterations. At each stage we should analyze linearly the stresses and strains by using the stiffness matrices and temperature forces which result from strains, stresses and secant reduction factors obtained at a previous stage. In this case the reduced stiffnesses of a buckled composite skin (E_x^s, E_y^s, G^s, ν_x^s, $\nu_y^s = \nu_x^s E_y^s / E_x^s$) with and without temperature variation consideration depend on the "supercritical strain" of a particular finite element, and one should rely on relations of [2] and [1], respectively.

At the initial iteration we solve the usual elastic problem for the structure with no skin buckling. Iterations stop when difference of stresses as obtained at two sequential iterations becomes rather small. In particular, if an unbuckled metal skin is involved in plastic deformation the present iterative process coincides with the traditional variable stiffness method [6] for physically nonlinear problems. The new method has been implemented in a computer program and validated by using example problems for which theoretical and numerical solutions have been provided elsewhere. New numerical analysis results are rather verisimilar and close to experimental data.

One knows two methods for finite-element modeling of a stiffened structure with a buckled skin. The first method is to prepare a rather dense mesh whose characteristic step sizes ℓ_1 and ℓ_2 are close to the stiffener spacing, to use the rod elements for modeling of stiffeners, and to introduce unstiffened plane-stress plates (with $F_1 = F_2 = 0$ in (1.23) and (1.24)) for modeling of skin cells. The second method is suitable for analyzing structures

with numerous stiffeners; here, use is made of the built-up finite elements described above, whose dimensions are much greater than ℓ_1 and ℓ_2; this enables analysts to increase the characteristic element dimensions to the distance between primary load-bearing components such as spars and frames. Of course, the second approach requires much less computation time and computer memory space and would be preferred.

Consider an example: nonlinear analysis of an edge-clamped cylindrical stiffened shell loaded with a transverse shear force. Structural dimensions and the value of the force may be seen in Fig. 1.17. This example is typical of real fuselages. Results of experiments with the present shell are reported in [8]. The skin is very thin (δ =0.51 mm), and its cells are subjected to various combinations of normal and shear stresses which lead the skin to buckling nonuniform over the cross section contour.

Analyses were carried out by using the nonlinear FEM program above. Introduced as nodal points of the finite-element mesh were points of intersection of longitudinal and transverse stiffeners. Stringers and frames were modeled with beam-type finite elements, and the skin, with flat quadrilateral membranes. Thus, the finite element for the skin models a real skin cell between neighboring stringers and frames. The FE model includes 126 nodal points with the total of 630 unknown displacements. At each iteration the program corrected the stiffnesses of element that model the shell skin: initial elastic properties of the skin material were multiplied by current values of reduction factors. The reduction factors for the skin under multiaxial load were computed by employing the method of [1].

Figure 1.18 depicts stress diagrams for the skin and stiffeners at the clamped end. Also, one can see experimentally obtained results from [8]. Comparison for the compression-loaded domain shows that data of experiments and the nonlinear analysis are in a rather good agreement.

Figure 1.19 represents diagrams of normal stresses as computed for stiffeners at the clamped end by using linear and nonlinear theories. It is clear that stresses differ much, especially in the compression-loaded domain. As compared with the linear calculation, the mean normal stress in the skin over the severest compression area has decreased by a factor of over 2.3, whereas stiffener stresses in the same area have been higher by 23%.

Part 2. Evaluating the effect of skin postbuckling behavior on general stability of a composite structure

2.1. Tangential stiffnesses of stiffened structure upon general buckling

In Part 1, we dealt with analysis of stresses and strains in a stiffened structure whose thin composite skin carries loads while being buckled. At a certain value of the external load global instability may occur. At that moment both the stresses and strains show small increments which may be regarded as variations to initial (subcritical) values for the structure with nonlinear dependence of strains on skin stresses.

In [1] the nonlinear dependence for a composite plate has been written as,

$$e_x = \frac{p_x}{E_x} - \mu_{yx}\frac{p_y}{E_y} + B_e(p,s), \quad e_y = \frac{p_y}{E_y} - \mu_{xy}\frac{p_x}{E_x} + \alpha_a{}^2 B_e(p,s),$$
$$\gamma = \frac{s}{G_{xy}} + B_\theta(p,s), \tag{2.1}$$

where $\alpha_a = a/b$ and $p = p_x + \alpha_a^2 p_y$.

The relations (2.1) were obtained by assuming proportional loading — that is, at $p = p^* \cdot t$ and $s = s^* \cdot t$, where t is the load parameter ($t \geq 1$) and $\{p^*, s^*\}$ is the critical load combination (refer to Fig. 2.1). Functions $B_e(p,s)$ and $B_\theta(p,s)$ in (2.1) represent the fact that upon local buckling the initially orthotropic plate becomes anisotropic at $s \neq 0$.

Variations to the initial relations (2.1) look like this:

$$\delta e_x = a^t_{11}\delta p_x + a^t_{12}\delta p_y + a^t_{13}\delta s,$$
$$\delta e_y = a^t_{21}\delta p_x + a^t_{22}\delta p_y + a^t_{23}\delta s, \tag{2.2}$$
$$\delta \gamma = a^t_{31}\delta p_x + a^t_{32}\delta p_y + a^t_{33}\delta s,$$

Here,

$$a^t_{11} = \frac{1}{E_x} + \frac{\partial B_e}{\partial p}, \quad a^t_{12} = a^t_{21} = -\frac{\mu_{xy}}{E_x} + \alpha_a^2\frac{\partial B_e}{\partial p}, \quad a^t_{13} = \frac{\partial B_e}{\partial s},$$
$$a^t_{22} = \frac{1}{E_y} + \alpha_a^4\frac{\partial B_e}{\partial p}, \quad a^t_{33} = \frac{1}{G_{xy}} + \frac{\partial B_\theta}{\partial s}, \quad a^t_{23} = \alpha_a^2\frac{\partial B_e}{\partial s},$$
$$a^t_{31} = \frac{\partial B_\theta}{\partial p}, \quad a^t_{32} = \alpha_a^2\frac{\partial B_\theta}{\partial p},$$

Potentiality conditions require that $a^t_{13} = a^t_{31}$ and $a^t_{23} = a^t_{32}$; this means that $\frac{\partial B_e}{\partial s} \equiv \frac{\partial B_\theta}{\partial p}$.

The latter condition will be met if the loading is proportional and the ratio of supercritical out-of-plane displacements, $\psi = f_{22}/f_{11}$, does not depend on the "supercriticality index" t; i.e.,

$$\psi = \frac{\bar{s}^*}{4 - \bar{p}^*}, \tag{2.3}$$

where $\bar{p}^* = p^*/p^*_{x0}$ and $\bar{s}^* = s^*/s^*_0$. In this case

$$B_e = \frac{\pi^2}{8a^2} f_{11}^2 (1 + 4\psi^2), \quad B_\theta = 4\frac{p^*_{x0}}{s^*_0} B_e \psi, \tag{2.4}$$

and

$$f_{11}^2 = \frac{\bar{p} - 1 + 4\psi\bar{s}}{\frac{1}{16}C_7 - \psi^2 C_8}, \quad \bar{p} = \frac{p}{p^*_{x0}}, \quad \bar{s} = \frac{s}{s^*_0}$$

Expressions for C_7 and C_8 are provided in [1].

Let us symbolize derivatives of B_e and B_θ with respect to p and s as follows:

$$B_{e,p} = \frac{\partial B_e}{\partial p}, \quad B_{e,s} = \frac{\partial B_e}{\partial s}, \quad B_{\theta,p} = \frac{\partial B_\theta}{\partial p}, \quad B_{\theta,s} = \frac{\partial B_\theta}{\partial s}. \tag{2.5}$$

Then we take into account (2.3) and (2.4) to obtain:

$$\begin{aligned} B_{e,p} &= \frac{1}{p^*_{x0}} \cdot \frac{\pi^2}{8a^2} \cdot \frac{1 + 4\psi^2}{\frac{1}{16}C_7 - \psi^2 C_8}, \quad B_{e,s} = \frac{1}{s^*_0} \cdot \frac{\pi^2}{2a^2} \cdot \frac{1 + 4\psi^2}{\frac{1}{16}C_7 - \psi^2 C_8} \cdot \psi = B_{\theta,p}, \\ B_{e,s} &= \frac{1}{s^*_0} \cdot \frac{p^*_{x0}}{s^*_0} \cdot \frac{2\pi^2}{a^2} \cdot \frac{1 + 4\psi^2}{\frac{1}{16}C_7 - \psi^2 C_8} \psi^2. \end{aligned} \tag{2.6}$$

With (2.4) and (2.5) written and the stability boundary equation being $\bar{p}^* + 4\psi\bar{s}^* = 1$, the original expressions (2.1) may be re-written in the form usual in studies on anisotropic materials:

$$\begin{aligned} e_x &= a^s_{11} p_x + a^s_{12} p_y + a^s_{13} s, \\ e_y &= a^s_{21} p_x + a^s_{22} p_y + a^s_{23} s, \\ \gamma &= a^s_{31} p_x + a^s_{32} p_y + a^s_{33} s, \end{aligned} \tag{2.7}$$

where

$$a^s_{11} = \frac{1}{E_x} + B_{e,p}\left(1 - \frac{p^*}{p}\right), \quad a^s_{12} = a^s_{21} = -\frac{\mu_{xy}}{E_x} + \alpha_a^2 B_{e,p}\left(1 - \frac{p^*}{p}\right),$$

$$a^s_{13} = a^s_{31} = B_{e,s}\left(1 - \frac{s^*}{s}\right), \quad a^s_{23} = a^s_{32} = \alpha_a^2 B_{e,s}\left(1 - \frac{s^*}{s}\right),$$

$$a^s_{33} = \frac{1}{G_{xy}} + \left(1 - \frac{s^*}{s}\right) \cdot \left(B_{\theta,s} - B_{e,s}\frac{p^*}{s^*}\right).$$

However, analyses are easier to perform upon transforming the relation (2.1) to the version corresponding to a quasi-isotropic material with variable elasticity parameters:

$$e_x = \left(\frac{1}{E_x} + \frac{B_e}{p}\right) p_x + \left(-\frac{\mu_{yx}}{E_y} + \alpha_a^2 \frac{B_e}{p}\right) p_y,$$
$$e_y = \left(-\frac{\mu_{xy}}{E_x} + \alpha_a^2 \frac{B_e}{p}\right) p_x + \left(\frac{1}{E_y} + \alpha_a^4 \frac{B_e}{p}\right) p_y, \qquad (2.8)$$
$$\gamma = \left(\frac{1}{G_{xy}} + \frac{B_\theta}{s}\right) s.$$

As for secant reduction factors (φ_x^s, φ_y^s, φ_γ^s) and the secant Poisson's ratio, the formulas derived in [1] are valid.

Also, (2.2) may be re-written to the form usual in studies on orthotropic materials with variable elasticity parameters. Loading is assumed to be proportional, so $\delta p_x = p_x^* \delta t$, $\delta p_y = p_y^* \delta t$, and $\delta s = s^* \delta t$; for $p^* \neq 0$ and $s^* \neq 0$ we obtain:

$$\delta e_x = \left(a_{11}^t + a_{13}^t \frac{s^*}{p^*}\right) \delta p_x + \left(a_{12}^t + \alpha_a^2 a_{13}^t \frac{s^*}{p^*}\right) \delta p_y,$$
$$\delta e_y = \left(a_{12}^t + \alpha_a^2 a_{13}^t \frac{s^*}{p^*}\right) \delta p_x + \left(a_{22}^t + \alpha_a^4 a_{13}^t \frac{s^*}{p^*}\right) \delta p_y, \qquad (2.9)$$
$$\delta\gamma = \left(a_{33}^t + a_{13}^t \frac{p^*}{s^*}\right) \delta s.$$

Then the stress increment expressions which are inverse to (2.9) become

$$\delta p_x = \frac{E_x^t}{1 - \mu_{xy}^t \mu_{yx}^t}\left(\delta e_x + \mu_{yx}^t \delta e_y\right), \quad \delta p_y = \frac{E_y^t}{1 - \mu_{xy}^t \mu_{yx}^t}\left(\delta e_y + \mu_{xy}^t \delta e_x\right), \delta s = G_{xy}^t \delta\gamma,$$

where

$$E_x^t = \frac{1}{a_{11}^t + a_{13}^t \frac{s^*}{p^*}}, \quad \mu_{yx}^t = -\frac{a_{12}^t + \alpha_a^2 a_{13}^t \frac{s^*}{p^*}}{\left(a_{11}^t + a_{13}^t \frac{s^*}{p^*}\right)}, \quad \mu_{xy}^t = -\frac{a_{12}^t + \alpha_a^2 a_{13}^t \frac{s^*}{p^*}}{\left(a_{22}^t + \alpha_a^4 a_{13}^t \frac{s^*}{p^*}\right)}, \qquad (2.10)$$
$$E_y^t = \frac{1}{a_{22}^t + \alpha_a^4 a_{13}^t \frac{s^*}{p^*}}, \quad G_{xy}^t = \frac{1}{a_{33}^t + a_{13}^t \frac{p^*}{s^*}}.$$

We proceed from relations $E_x^t = E_x \varphi_x^t$, $E_y^t = E_y \varphi_y^t$, and $G_{xy}^t = G_{xy} \varphi_\gamma^t$; relevant reduction factors may be determined from (2.10).

For increments of stress resultants and moments upon global buckling the following equations are valid:

$$N_x = \int_h \delta p_x \, dz, \quad N_y = \int_h \delta p_y \, dz, \quad N_{xy} = \int_h \delta s \, dz,$$

$$M_x = \int_h \delta p_x \, z dz, \quad M_y = \int_h \delta p_y \, z dz, \quad M_{xy} = \int_h \delta s \, z dz.$$

Now we can employ the Kirchhoff-Love hypothesis and the Shanley hypothesis on loading continuation at bifurcation; with this, the latter equations provide the following expressions for reduced tangential stiffnesses of the skin:

$$B^t_{110} = \frac{E^t_x h}{1-\mu^t_{xy}\mu^t_{yx}}, \quad B^t_{220} = \frac{E^t_y h}{1-\mu^t_{xy}\mu^t_{yx}}, \quad B^t_{330} = G^t_{xy} h, \quad B^t_{120} = \frac{\mu^t_{yx} E^t_x h}{1-\mu^t_{xy}\mu^t_{yx}}$$

$$D^t_{110} = \frac{E^t_x h^3}{12\left(1-\mu^t_{xy}\mu^t_{yx}\right)}, \quad D^t_{220} = \frac{E^t_y h^3}{12\left(1-\mu^t_{xy}\mu^t_{yx}\right)}, \quad D^t_{330} = \frac{G^t_{xy} h^3}{12}, \quad D^t_{120} = \mu^t_{yx} D^t_{110}. \tag{2.11}$$

If the skin is stiffened regularly with longitudinal and transverse elements (having spacings b_s and b_f, respectively) then the tangential stiffnesses of the stiffened panel are similar to (2.11):

$$B^t_{11} = E_s\left(r_{ts} h + \frac{F_s}{b_s}\right), \quad B^t_{22} = E_f\left(r_{tf} h + \frac{F_f}{b_f}\right), \quad B^t_{33} = \left(G^t_{xy} h + G^t_{sf} h_{sf}\right),$$

$$B^t_{12} = B^t_{120}, \quad B^t_3 = B^t_{330} + B^t_{120},$$

$$D^t_{11} = E_s\left[r_{ts}\left(\frac{h^3}{12} + h h_1^2\right) + \frac{I_s}{b_s} + \frac{F_c}{b_s}\left(z_s - h_1\right)^2\right], \tag{2.12}$$

$$D^t_{22} = E_f\left[r_{tf}\left(\frac{h^3}{12} + h h_2^2\right) + \frac{I_f}{b_f} + \frac{F_f}{b_f}\left(z_f - h_2\right)^2\right], \quad D^t_{33} = G^t_{xy}\frac{h^3}{6},$$

$$D^t_3 = 2D^t_{330} + D^t_{120} + \frac{G_s I^P_s}{2b_s} + \frac{G_f I^P_f}{2b_f}.$$

where

$$r_{ts} = \frac{E^t_x}{E_s\left(1-\mu^t_{xy}\mu^t_{yx}\right)}, \quad r_{tf} = \frac{E^t_y}{E_f\left(1-\mu^t_{xy}\mu^t_{yx}\right)}$$

E_s, E_f, G_s, and G_f are elastic moduli and shear moduli of the longitudinal and transverse elements,

$F_s, F_f, I_s, I_f, I^P_s$, and I^P_f are cross-sectional areas, central moments of inertia, and the product of inertia of the longitudinal and transverse elements, respectively,

z_s and z_f are distances from the skin midsurface to centroids of the longitudinal and transverse elements, respectively,

h_1 and h_2 are distances from the skin midsurface to centroids of the longitudinal and transverse elements with relevant skin strips, respectively, and

$G_{sf} \cdot h_{sf}$ is the shear stiffness of the frames/spars with no skin; this value depends on a method for joining the longitudinal and transverse frames/spars.

These equations for secant and tangential stiffness parameters are used hereinafter to analyze subcritical stresses and strains and general stability of the stiffened structure. In the case with no skin buckling the equations become the traditional expressions for stiffnesses of a stiffened panel.

2.2. Stability of regularly stiffened cylindrical and flat composite panels and shells in the case of uniform loading with compression and shear

Consideration now is given to a stiffened cylindrical panel whose radius is R and planform dimensions are A and B (see Fig. 2.2). The panel is regularly stiffened with longitudinal and transverse elements. The cross-sectional area and the spacing of longitudinal element are F_s and b_s, respectively; and those of transverse elements are F_f and b_f, respectively. It is assumed that the panel skin is a thin composite with layup sequence being symmetric with respect to the skin midsurface. Reduced mechanical characteristics of the skin correspond to characteristics of a homogeneous orthotropic material — E_x, E_y, G_{xy}, μ_{xy}, μ_{yx} ($E_x\mu_{yx} = E_y\mu_{xy}$). The skin thickness is h. Dimensions b_s and b_f are much lower than A and B, so the skin cell may be assumed to be flat.

Let us use u, v, and w to denote projections (on axes x, y, and z, respectively) of a small displacement of a panel point.

For a shallow panel either stiffened or unstiffened being uniformly loaded with stress resultants N_x^0, N_y^0, and N_{xy}^0 (with no moments applied) and unbuckled, we can write the following linear equations:

$$[\bar{L}]\{U\} = 0, \tag{2.13}$$

Here, $[\bar{L}]$ is a symmetric 3 by 3 matrix whose components are differential operators

L_{ij} for stability equations (i, j = 1, 2, 3) and

$\{U\}$ is the displacement vector with components u, v, and w.

The differential operators in (2.13) have the following form (as provided in [9]):

$$L_{11} = B_{11}^t \frac{\partial^2}{\partial x^2} + B_{33}^t \frac{\partial^2}{\partial y^2}, \quad L_{12} = L_{21} = B_3^t \frac{\partial^2}{\partial x \partial y},$$

$$L_{13} = L_{31} = -\frac{B_{12}^t}{R}\frac{\partial}{\partial x}, \quad L_{22} = B_{22}^t \frac{\partial^2}{\partial y^2} + B_{33}^t \frac{\partial^2}{\partial x^2}, \quad L_{23} = L_{32} = -\frac{B_{22}^t}{R}\frac{\partial}{\partial s}, \qquad (2.14)$$

$$L_{33} = D_{11}^t \frac{\partial^4}{\partial x^4} + 2D_3^t \frac{\partial^4}{\partial x^2 \partial y^2} + D_{22}^t\left(\frac{\partial^4}{\partial s^4} + \frac{2}{R^2}\frac{\partial^2}{\partial s^2} + \frac{1}{R^4}\right) + \frac{B_{22}^t}{R} -$$

$$- N_x^0 \frac{\partial^2}{\partial x^2} - 2N_{xy}^0 \frac{\partial^2}{\partial x \partial y} - N_y^0 \frac{\partial^2}{\partial y^2}.$$

In the case of a panel whose edges $x=0$, $x=A$, $y=0$, and $y=B$ are freely supported, the solution to (2.13) may be written as

$$u = \sum_{n=1}^{\infty}\sum_{m=1}^{\infty} A_{mn} \cos\frac{m\pi x}{A}\sin\frac{n\pi y}{B}, \quad v = \sum_{n=1}^{\infty}\sum_{m=1}^{\infty} B_{mn} \sin\frac{m\pi x}{A}\cos\frac{n\pi y}{B},$$
$$w = \sum_{n=1}^{\infty}\sum_{m=1}^{\infty} C_{mn} \sin\frac{m\pi x}{A}\sin\frac{n\pi y}{B}. \qquad (2.15)$$

Upon substituting relations (2.15) into (2.13) and resorting to the Bubnov-Galerkin method we obtain an infinite homogeneous algebraic system of linear equations for the constants C_{mn}:

$$C_{mn}\left[\frac{(c_{11}c_{23} - c_{13}c_{22})c_{31} + (c_{13}c_{21} - c_{11}c_{23})c_{32}}{c_{11}c_{22} - c_{12}^2} + c_{33} - p_g\right] =$$
$$= \frac{32\alpha mns_g}{\pi^2}\sum_r\sum_s C_{rs}\frac{rs}{(m^2 - r^2)(n^2 - s^2)}, \qquad (2.16)$$

where m, n, r, s = 1, 2, 3, ...∞ and the values of m+r and n+s are odd numbers,

$$c_{11} = m^2 + b_{12}n^2\alpha^2, \quad c_{12} = c_{21} = b_3 mn\alpha, \quad c_{13} = c_{31} = b_{12}m\beta,$$
$$c_{23} = c_{32} = b_{22}n\alpha\beta, \quad c_{33} = \pi^2\left[d_{11}m^4 + 2d_3m^2n^2\alpha^2 + d_{22}\left(n^2\alpha^2 - \beta^2\right)^2\right] + b_{22}\beta^2, \qquad (2.17)$$

$$p_g = \frac{N_x^0}{B_{11}^t}m^2 + \frac{N_y^0}{B_{11}^t}n^2\alpha^2, \quad s_g = \frac{N_{xy}^0}{B_{11}^t},$$
$$\alpha = \frac{A}{B}, \quad \beta = \frac{A}{\pi R}, \quad b_{ij} = \frac{B_{ij}^t}{B_{11}^t}, \quad d_{ij} = \frac{D_{ij}^t}{B_{11}^t A^2}.$$

The stress resultants N_x^0, N_y^0, and N_{xy}^0 are assumed to be proportional to a single parameter t; one could limit the system (2.16) with a certain set of equations (it suffices to adopt m and n of 6 to 8); with this, it is easy to establish the critical value $t = t^*$ which zeros the system (2.16) determinant.

The global stability analysis is performed in compliance with the algorithm depicted in Fig. 1.15:

— the load parameter is incremented from zero in steps of Δt;

— at each load step the iterative procedure is run in order to determine subcritical stresses and strains in both the skin and stiffeners;

— if the skin is to buckle at the current load level, then relations (2.10) and (2.12) are employed to establish tangential stiffnesses of the panel and their respective determinant of the system (2.16);

— if the system (2.16) determinant changes its sign at a certain load level, then the critical value of t^* should be refined to the accuracy required.

The problem of general stability of a stiffened circular cylindrical shell (Fig. 2.3) is solved in a similar way. A particular solution to the system (2.13) is represented by,

$$u = A\cos(\lambda_m \bar{x} - n\varphi), \quad v = B\cos(\lambda_m \bar{x} - n\varphi), \quad w = C\sin(\lambda_m \bar{x} - n\varphi), \qquad (2.18)$$

where $\bar{x} = x / \ell$, $\varphi = s / R$,

ℓ is a shell half-length,

s is a cross section point coordinate measured along the circle,

λ_m and n are wave parameters.

By substituting (2.18) into (2.13) at a fixed value of n and performing the necessary mathematical manipulations we arrive at the characteristic algebraic equation of the eighth order with respect to λ_m; roots of this equation taken together with the eight constants C_m ($m = 1, 2, \ldots, 8$) make it possible to write the general solution to (2.13):

$$w = \sum_{m=1}^{8} C_m \sin(\lambda_m \bar{x} - n\varphi). \qquad (2.19)$$

Constants A_m and B_m are functions of C_m.

Boundary conditions for shell ends $\{ x = \pm\ell \}$ are the following:

$w = \dfrac{\partial^2 w}{\partial x^2} = N_x = v = 0$ in the case of free support at the ends,

$w = \dfrac{\partial w}{\partial x} = N_x = v = 0$ in the case of clamping of the ends.

These allow one to formulate 8 linear homogeneous algebraic equations for constants C_m. Coefficients of these equations depend on shell end loads N_x^0, N_s^0, and N_{xs}^0. The condition of existence of a nontrivial solution to the system provides the critical load parameter value t^* and the critical load $\{ N_x^*, N_s^*, N_{xs}^* \}$ of global buckling.

Let us delve into particular problems with stiffened structures whose skins buckle and carry loads upon buckling until the structure undergoes global buckling.

The initiatory problem is on a flat (1/R=0) stiffened panel with planform dimensions A=480 mm and B=400 mm. The skin with the thickness of 2.64 mm is made out of a composite with the following equivalent characteristics: $E_x = 6682\,\text{kg/sq.mm}$, $E_y = 3768\,\text{kg/sq.mm}$, $G_{xy} = 1434\,\text{kg/sq.mm}$, $\mu_{xy} = 0.32$. Ultimate stresses of the skin are $\sigma_x^c = 44.5\,\text{kg/sq.mm}$ in compression, $\sigma_x^t = 31.2\,\text{kg/sq.mm}$ in tension, and $\tau^{sh} = 24.8\,\text{kg/sq.mm}$ in shear. Longitudinal and transverse stiffeners are rectangular shapes with cross-sectional sizes 20 by 5 mm and the spacing steps $b_s = 100\,\text{mm}$ and $b_f = 120\,\text{mm}$. Stiffener material characteristics are as follows: the Young modulus E=8346 k g/sq.mm, the compressive strength $\sigma^c = 55.5\,\text{kg/sq.mm}$, and the tensile strength $\sigma^t = 39.0\,\text{kg/sq.mm}$.

Critical stresses of local buckling of a skin cell between stiffeners in the case of uniaxial loading are $p_{x0}^* = 10.87\,\text{kg/sq.mm}$, $p_{y0}^* = 7.55\,\text{kg/sq.mm}$ and $s_0^* = 21.29\,\text{kg/sq.mm}$.

Figures 2.4 and 2.5 show the analytical results. More particularly, Fig. 2.4represents the global buckling boundary curve in the plane $\{N_x^0, N_{xy}^0\}$ (note that $N_y^0 = 0$); it defines the critical load combination $\{N_x^*, N_{xy}^*\}$ (shown by the solid line) and has been drawn with consideration of skin postbuckling behavior (until the panel becomes buckled) for the following load combinations:

$$\frac{N_{xy}^0}{N_x^0} = 0,\ 0.2,\ 0.4,\ 0.6,\ 0.8,\ 1.0 \quad \text{and} \quad \frac{N_x^0}{N_{xy}^0} = 1.0,\ 0.8,\ 0.6,\ 0.4,\ 0.2,\ 0.$$

Also, one sees here a similar kind of boundary curves computed for the same panel without assuming the skin to carry loads upon local buckling (the dashed line). By comparing these curves it is clear that the global stability analysis with no correction for load-carrying capability of the buckled skin may be misleading in its overestimating the global buckling load by 25% to 60%.

Figure 2.5 represents stresses in components of the stiffened panel being in subcritical state, immediately before global buckling; consideration is given to all the above-mentioned combinations of shear and compressive loads at the edges. Here, solid lines are for component stresses if the analysis takes into account load-carrying capability of the buckled skin, and dashed lines, for component stresses calculated with no account of load-carrying capability of the buckled skin. In case the shear load is relatively low the most notable difference is between mean stresses in the buckled skin, p_x, and the nominal skin stress σ_x if the analysis does not allow for early skin buckling. When the shear load is great, one could reveal additional compression of both longitudinal and transverse stiffeners which

is caused by appearance of oblique waves in the skin — see σ_s and σ_f in Fig. 2.5 for $N_x^0 \to 0$ at $N_{xy}^0 \neq 0$.

However, it should be noticed that, when the shear load is increased,the mean shear stress $s\_$ in the skin grows rather rapidly and reachesthe ultimate level $\left(\tau^{sh} \approx 25\,\text{kg / sq. mm}\right)$ at $N_{xy}^0 \approx 72\,\text{kg / mm}$. Thus, if the shear stress resultant N_{xy}^0 is higher than 72 kg/mm, we should expect the skin to break at loads less than the global instability load.

Consider also analysis of global stability of a stiffened cylindrical panel with radius R=1270 mm. Panel planform dimensions, longitudinal and transverse stiffener shape and sizes, skin thickness and material characteristics are the same as those of the flat plate above.

Figure 2.4 demonstrates the panel buckling boundary computed by the present method. Clearly, the panel curvature does notably improve general stability. Calculation for the same panel with no allowance for buckled skin stiffness provides results which are greatly overstated — by 20% to 40%.

Consider now the problem of stability of stiffened circular cylindrical shell subjected to torsion. The shell has the following main parameters: curvature radius R=750 mm, overall length $2\ell = 2100\,\text{mm}$, skin thickness h=1 mm. The skin is regularly stiffened with stringers (with the spacing $b_s = 118\,\text{mm}$) and frames (with the spacing $b_f = 150\,\text{mm}$). The stringers are rectangular 8 mm by 20 mm shapes, and frames are angles with leg sizes of 15 mm and 35 mm and the web thickness of 2.0 mm. The material of both the skin and stiffeners is isotropic, E=7200 kg/sq.mm and $\mu = 0.33$.

Three identical metal shells have been manufactured and tested under torsion. At skin stresses $\tau \approx 4.8\,\text{kg/sq. mm}$ the skin had buckled and remained in this state until the shell failed due to its global buckling. Figure 2.6 demonstrates one of the shells in a subcritical state (as for global buckling). One can readily see local waves in skin cells. Here, the "supercriticality level" is approximately 3. Figure 2.7 represents global buckling of the shell; spiral waves involve stringers and frames into large deformation. The experiments provided the following values of critical shear for the three shells tested:

$$N^*_{xy(1)} = 14.2\,\text{kg/mm},\ N^*_{xy(2)} = 13.8\,\text{kg/mm},\ N^*_{xy(3)} = 13.7\,\text{kg/mm}.$$

Our analyses with postbuckling skin stiffness reduction suggest $N^*_{xy} = 15\,\text{kg/mm}$. Thus, the experimental data are at the level of 91% - 95% of the theory. In contrast, analysis of the same shells with no allowance for stiffness reduction overstates the critical load by approximately 35%.

2.3 Analyzing the stability of a built-up cylindrical structure with consideration of global and local buckling, nonuniform loading and buckled-skin load-bearing capability

Below, we describe a high-accuracy numerical method for analyzing stability of built-up composite/metal structures subjected to subcritical loading with compressive and shear forces which vary along the cross section contour.

The structure is a cylindrical or slightly conical system of interacting rods, plates and shells made of composites or metals and subjected to mechanical and thermal loads.

Account is taken of variable curvature, loads, thickness, initial out-of-plane displacements, and subcritical deformation of the system along the contour. Also, the skin is assumed to be multi-layered; elements, anisotropic; stiffeners, discrete; and global/local buckling, likely.

The method is based on

— formulating the corresponding homogeneous boundary-value problem,

— separating the problem variables, and

— solving numerically the stability equations for the structural elements by means of the discrete orthogonalization method of [10].

Of course, all the structural components are linked into a system by using finite element methods.

Consider an isolated anisotropic non-circular cylindrical shell that in the subcritical state is loaded with stress resultants $N_x^0(s,t)$, $N_s^0(s,t)$, and $N_{xs}^0(s,t)$ (Fig. 2.8) where t is the load growth parameter, $t \geq 0$. General equations of structural stability which describe buckling of the shell may be represented as three groups of relations (refer to [4]).

I. Neutral equilibrium equations:

$$\frac{\partial N_x}{\partial x}+\frac{\partial S}{\partial s}=-\frac{\partial}{\partial x}\left(N_x^0\frac{\partial u}{\partial x}+N_{xs}^0\frac{\partial u}{\partial s}\right)-\frac{\partial}{\partial s}\left(N_{sx}^0\frac{\partial u}{\partial x}+N_s^0\frac{\partial u}{\partial s}\right),$$

$$\frac{\partial N_s}{\partial s}+\frac{\partial S}{\partial x}+\frac{1}{R}\frac{\partial M_{sx}}{\partial x}+\frac{Q_s}{R}=-\frac{\partial}{\partial x}\left[N_x^0\frac{\partial v}{\partial x}+N_{xs}^0\left(\frac{\partial v}{\partial s}+\frac{w}{R}\right)\right]-\frac{\partial}{\partial s}\left[N_{sx}^0\frac{\partial v}{\partial x}+N_s^0\left(\frac{\partial v}{\partial s}+\frac{w}{R}\right)\right]$$

$$\frac{N_s}{R}-\frac{\partial Q_x}{\partial x}-\frac{\partial Q_s}{\partial s}=-\frac{N_{sx}^0}{R}\frac{\partial v}{\partial x}-\frac{N_s^0}{R}\left(\frac{\partial v}{\partial s}+\frac{w}{R}\right), \qquad (2.20)$$

$$Q_x=\frac{\partial M_x}{\partial x}+\frac{\partial M_{sx}}{\partial s}-N_x^0\theta_x-N_{xs}^0\theta_s-\left(\theta_s^0+\theta_0\right)S,$$

$$Q_s=\frac{\partial M_s}{\partial s}+\frac{\partial M_{xs}}{\partial x}-N_s^0\theta_s-N_{sx}^0\theta_x-\left(\theta_s^0+\theta_0\right)N_s,$$

$$\left(S=N_{xs}-\frac{M_{sx}}{R}=N_{sx},\ H=\frac{1}{2}\left(M_{xs}+M_{sx}\right)\right).$$

II. Elasticity relations (from [11, 12]):

$$\begin{Bmatrix}\{N\}\\ \{M\}\end{Bmatrix}=\begin{bmatrix}[B] & [C]\\ [C] & [D]\end{bmatrix}\begin{Bmatrix}\{\varepsilon\}\\ \{æ\}\end{Bmatrix}. \tag{2.21}$$

Here, the meaning of new symbols is as follows:

$$\{N\}=\lfloor N_x\ N_s\ S\rfloor^T,\quad \{M\}=\lfloor M_x\ M_s\ H\rfloor^T,\quad \{\varepsilon\}=\lfloor \varepsilon_x\ \varepsilon_s\ \gamma_{xs}\rfloor^T,$$
$$\{æ\}=\lfloor æ_x\ æ_s\ æ_{xs}\rfloor^T,\quad [B]=\left[B_{ij}\right]=[B]^T,\quad [C]=\left[C_{ij}\right]=[C]^T,$$
$$[D]=\left[D_{ij}\right]=[D]^T,\ i,j=1,2,3.$$

III. Geometric interrelations:

$$\varepsilon_x=\frac{\partial u}{\partial x},\quad \varepsilon_s=\frac{\partial v}{\partial s}+\frac{w}{R}+\underline{\underline{\left(\theta_s^0+\theta_0\right)\theta_s}},$$
$$\gamma_{xs}=\frac{\partial u}{\partial s}+\frac{\partial v}{\partial x}+\underline{\underline{\left(\theta_s^0+\theta_0\right)\theta_x}},$$
$$æ_x=\frac{\partial \theta_x}{\partial x},\quad æ_s=\frac{\partial \theta_s}{\partial s},\quad æ_{xs}=\frac{\partial \theta_s}{\partial x}=\frac{\partial \theta_x}{\partial s}+\underline{\frac{1}{R}\frac{\partial v}{\partial x}}, \tag{2.22}$$
$$\theta_x=-\frac{\partial w}{\partial x},\quad \theta_s=-\frac{\partial w}{\partial s}+\underline{\frac{v}{R}},\qquad \left(\theta_0=-\frac{dw_0}{ds},\quad \theta_s^0=-\frac{dw^0}{ds}+\underline{\frac{v^0}{R}}\right).$$

Hereafter,

u, v, w, θ_x, and θ_s are additional linear displacements and rotation angles of the normal to the skin;

ε_x, ε_s, γ_{xs}, $æ_x$, $æ_s$, and $æ_{xs}$ are strains and curvature variation components;

$w_0(s)$ and $w^0(s)$ are initial and "accumulated" subcritical out-of-plane displacements; and

B_{ij}, C_{ij}, and D_{ij} (i, j=1, 2, 3) are shell stiffness parameters.

Boundary conditions for edges {s=0} and {s=b} of the isolated shell are described by,

$$w|_{s=0}\left(1-\gamma_0\right)+\overline{Q}_s|_{s=0}\gamma_0=0,\qquad w|_{s=b}\left(1-\gamma_1\right)+\overline{Q}_s|_{s=b}\gamma_1=0,$$
$$\theta_s|_{s=0}\left(1-\delta_0\right)+M_s|_{s=0}\delta_0=0,\qquad \theta_s|_{s=b}\left(1-\delta_1\right)+M_s|_{s=b}\delta_1=0,$$
$$u|_{s=0}\left(1-\varphi_0\right)+\overline{S}|_{s=0}\varphi_0=0,\qquad u|_{s=b}\left(1-\varphi_1\right)+\overline{S}|_{s=b}\varphi_1=0, \tag{2.23}$$
$$v|_{s=0}\left(1-\psi_0\right)+\overline{N}_s|_{s=0}\psi_0=0,\qquad v|_{s=b}\left(1-\psi_1\right)+\overline{N}_s|_{s=b}\psi_1=0,$$

Here, the constants γ_0, δ_0, φ_0, ψ_0, γ_1, δ_1, φ_1, and ψ_1 take the values 0 or 1 for cases with displacement control and load control, respectively. Lastly, additional symbols are,

$$\overline{S}=S+\underline{N_{sx}^0\frac{\partial u}{\partial x}+N_s^0\frac{\partial u}{\partial s}},\quad \overline{Q}_s=Q_s+\frac{\partial M_{sx}}{\partial x},$$
$$\overline{N}_s=N_s+\underline{N_{sx}^0\frac{\partial v}{\partial x}+N_s^0\left(\frac{\partial v}{\partial s}+\frac{w}{R}\right)}.$$

The critical value t_* of the load parameter t_- is sought to be the minimum value of t at which the homogeneous boundary-value problem (2.20) ÷ (2.23) has a non-zero solution (subjected to the extra condition of simple support at shell ends {x=0} and {x=a}). Underlined terms in the above equations provide options for analyzing general stability of the structure in combination with local and temperature-induced buckling.

Stability equations for a built-up stiffened cylindrical structure composed of interacting cylindrical shells, plates and rods may be written in a similar way. For instance, an i-th web (see Fig. 2.8) may be analyzed by employing relations similar to (2.20) – (2.23) in the local coordinate system $\{X_1, X_2, X_3\}$ which are provided in the work [13]; the latter also gives compatibility conditions for displacements in the skin and stiffeners. Stability equations for plates in the structure may be derived from (2.20) – (2.23) by assuming that 1/R=0.

All equations are written for each shell, plate and stiffeners. At all joints of shells and plates the equations are complemented with the fitting conditions which include equilibrium equations and the condition of generalized displacements being identical at each joint (refer to [13]). Free and supported longitudinal edges of some elements must meet the boundary conditions (2.23).

The major difference between the new system of homogeneous differential equations and the one in [13] is that the former system includes general elasticity relations (2.21) which are characteristic of anisotropic composite structures; this circumstance notably complicates solution procedures.

To begin with, we have to consider a particular problem with no subcritical shear load and no orthotropy in elements – more specifically, $N^0_{sx}=0$, $B_{13}=B_{23}=C_{13}=C_{23}=D_{13}=D_{23}=0$. The solution for each shell may be written as,

$$\{P\} = \{P_n\}\cos\frac{n\pi x}{a}, \quad \{F\} = \{F_n\}\sin\frac{n\pi x}{a}, \tag{2.24}$$

where

$$\{P\} = \lfloor u\ \theta_x\ \gamma_{xs}\ æ_{xs}\ S\ H\ Q_x \rfloor^T, \quad \{P_n\} = \lfloor u_n\ \theta_{xn}\ \gamma_n\ æ_{xsn}\ S_n\ H_n\ Q_{xn} \rfloor^T,$$

$$\{F\} = \lfloor v\ w\ \theta_s\ \varepsilon_x\ \varepsilon_s\ æ_x\ æ_s\ N_x\ N_s\ M_x\ M_s\ Q_s \rfloor^T,$$

$$\{F_n\} = \lfloor v_n\ w_n\ \theta_n\ \varepsilon_{xn}\ \varepsilon_n\ æ_{xn}\ æ_n\ N_{xn}\ N_n\ M_{xn}\ M_n\ Q_n \rfloor^T.$$

In addition, n is the number of longitudinal half-waves in the shell, and the functions with the subscript n are only depending on the coordinate s.

Stability equations (2.20) – (2.22) can in this case be transformed into the system of 8 ordinary differential equations (at any values of n and t as the work [13] states):

$$\frac{d\{u\}}{ds} = [\bar{C}]\{u\}, \tag{2.25}$$

Here,

$\{u\} = \lfloor w_n\ \theta_n\ M_n\ \overline{Q}_n\ u_n\ v_n\ \overline{N}_n\ \overline{S}_n \rfloor^T$ is the column vector to be sought,

$$\overline{S}_n = S_n + N_s^0 \frac{du_n}{ds}, \quad \overline{N}_n = N_n + N_s^0\left(\frac{dv_n}{ds} + \frac{w}{R}\right), \quad \overline{Q}_n = Q_n - \frac{n\pi}{a} H_n$$

$[\overline{C}]$ is the matrix whose coefficients are known functions of s.

Boundary conditions for an isolated element may be written as,

$$[\Gamma_0]\{u(0)\} = 0, \quad [\Gamma_1]\{u(b)\} = 0, \tag{2.26}$$

where $[\Gamma_0]$ and $[\Gamma_1]$ are constant 4 by 8 matrices.

The problem (2.25) – (2.26) may be efficiently solved by utilizing the discrete orthogonalization method (which requires solving some Cauchy problems). For a point {s=b} the solution is,

$$\{u(b)\} = [Z(b)]\{\overline{C}(b)\}$$

and the condition for obtaining the critical value t* is written as follows:

$$\det[\overline{D}(t)] = 0, \tag{2.27}$$

where $[\overline{D}] = [\Gamma_1][Z(b)]$ and $[Z(b)]$ is the established solution matrix.

To analyze a built-up cylindrical system, the following procedure is applicable. Solutions in the form of (2.24) are written for all elements. Equations (2.25) are obtained for each shell and plate while assuming the unit-displacement boundary condition – for example, for the following conditions at points $\{s^k = 0\}$ and $\{s^k = b^k\}$:

$$w_n^k\big|_{s^k=0} = 1, \quad \theta_n^k = u_n^k = v_n^k\big|_{s^k=0} = w_n^k = \theta_n^k = u_n^k = v_n^k\big|_{s^k=b^k} = 0.$$

Here, the superscript k is the identification number of the element. Proceeding in the same way, generalized stiffness matrices are established for each element $\left([K']^k\right)$ and the entire structure $([K])$; use is made of conventional algorithms of assumed-displacement finite element methods. The resulting equations for neutral equilibrium become linear algebraic equations (at any n and t):

$$[K]\{y\} = 0, \tag{2.28}$$

where {y} is the generalized displacement vector for all nodes in a cross section of the system. The vector comprises all nodal displacement vectors:

$$\{y_i\} = \lfloor w_{ni}\ \varphi_{ni}\ u_{ni}\ v_{ni} \rfloor^T, \quad i = 1, 2, \ldots, N$$

The equation for determining t_* takes the form,

$$\det[K(t)] = 0. \tag{2.29}$$

Initially, we should use (2.29) to find t_n at various values of n; thereafter, t_* is sought as $\min_n t_n$ at $n = n_*$. Finally, (2.28) is utilized to determine the eigenvector $\{y_*\}$ and the structure buckling shape.

In the general case the subcritical shear load is non-zero and/or elasticity relations (2.21) for at least one element have a general form; then the solution to the structural stability problem assumes a form differing from (2.24):

$$\{P\} = \{P_n\}\cos\frac{\pi x}{\ell} + \{\tilde{P}_n\}\sin\frac{\pi x}{\ell}, \quad \{F\} = \{F_n\}\sin\frac{\pi x}{\ell} + \{\tilde{F}_n\}\cos\frac{\pi x}{\ell}. \qquad (2.24')$$

Here, variables of the first group ($\{P_n\}$, and $\{F_n\}$) are the same as in (2.24), whereas variables of the second group are

$$\{\tilde{P}_n\} = \lfloor \tilde{u}_n\ \tilde{\theta}_{xn}\ \tilde{\gamma}_n\ \tilde{\text{æ}}_{xsn}\ \tilde{S}_n\ \tilde{H}_n\ \tilde{Q}_{xn} \rfloor^T,$$
$$\{\tilde{F}_n\} = \lfloor \tilde{v}_n\ \tilde{w}_n\ \tilde{\theta}_n\ \tilde{\varepsilon}_{xn}\ \tilde{\varepsilon}_n\ \tilde{\text{æ}}_{xn}\ \tilde{\text{æ}}_n\ \tilde{N}_{xn}\ \tilde{N}_n\ \tilde{M}_{xn}\ \tilde{M}_n\ \tilde{Q}_n \rfloor^T.$$

In this case the structure is assumed to be rather long; $\ell > 0$ denotes the buckling half-wave for the longitudinal direction (in practical analyses it suffices to adopt $\ell = \ell_n = a/n$, $n = 1, 2, 3, \ldots$).

Further, we can substitute (2.24') into shell stability equations (2.20) – (2.21) to separate the variables and obtain 16 simultaneous ordinary differential equations below (in which the prime sign symbolizes differentiation with respect to s; $\bar{\theta}_s^0 = \theta_s^0 + \theta_0$):

$$w_n' = -\theta_n + \frac{v_n}{R},$$

$$M_n' = \left(N_s^0 + N_s^0\bar{\theta}_s^{02}\right)\theta_n + \bar{Q}_n + 2\mu_n H_n + \bar{\theta}_s^0\bar{N}_n - N_s^0\bar{\theta}_s^0\varepsilon_n + \bar{\theta}_s^0 N_{sx}^0\mu_n\tilde{v}_n + N_{sx}^0\mu_n\tilde{w}_n,$$

$$\bar{Q}_n' = \mu_n^2\left(N_x^0 + N_s^0\bar{\theta}_s^{02}\right)w_n - \mu_n^2\bar{\theta}_s^0 N_s^0 v_n + \frac{\bar{N}_n}{R} - \mu_n\bar{\theta}_s^0\bar{S}_n + \mu_n\bar{\theta}_s^0 N_s^0\gamma_n + \mu_n^2 M_{xn} - \mu_n N_{xs}^0\tilde{\theta}_n + \mu_n^2 N_{xs}^0\bar{\theta}_s^0\tilde{u}_n,$$

$$u_n' = \gamma_n - \mu_n v_n + \bar{\theta}_s^0\mu_n w_n,$$

$$v_n' = \varepsilon_n - \frac{w_n}{R} - \bar{\theta}_s^0\theta_n,$$

$$\bar{N}_n' = -\mu_n^2 N_s^0\bar{\theta}_s^0 w_n - \frac{\bar{Q}_n}{R} + \mu_n^2\left(N_x^0 + N_s^0\right)v_n + \mu_n\bar{S}_n - \mu_n N_s^0\gamma_n + N_{sx}^0\mu_n\left(\tilde{\varepsilon}_n - \bar{\theta}_s^0\tilde{\theta}_n\right) - N_{sx}^0\mu_n^2\tilde{u}_n,$$

$$\bar{S}_n' = \mu_n^2 N_x^0 u_n - \mu_n N_{xn} - \mu_n N_{xs}^0\left(\tilde{\gamma}_n + \mu_n\tilde{v}_n - \bar{\theta}_s^0\mu_n\tilde{w}_n\right),$$

$$
\left.
\begin{aligned}
&\tilde{w}_n' = -\tilde{\theta}_n + \frac{\tilde{v}_n}{R},\\
&\tilde{\theta}_n' = \tilde{æ}_n,\\
&\tilde{M}_n' = \left(N_s^0 + N_s^0\bar{\theta}_s^{02}\right)\tilde{\theta}_n + \tilde{\bar{Q}}_n + \bar{\theta}_s^0\tilde{\bar{N}}_n - N_s^0\bar{\theta}_s^0\tilde{\varepsilon}_n - 2\mu_n\tilde{H}_n -\\
&\qquad - \bar{\theta}_s^0 N_{sx}^0\mu_n v_n - N_{sx}^0\mu_n w_n,\\
&\tilde{\bar{Q}}_n' = \mu_n^2\left(N_x^0 + N_s^0\bar{\theta}_s^{02}\right)\tilde{w}_n - \mu_n^2\bar{\theta}_s^0 N_s^0\tilde{v}_n + \frac{\tilde{\bar{N}}_n}{R} + \mu_n\bar{\theta}_s^0\tilde{\bar{S}}_n -\\
&- \mu_n\bar{\theta}_s^0 N_s^0\tilde{\gamma}_n + \mu_n^2\tilde{M}_{xn} + \mu_n N_{sx}^0\theta_n + \mu_n^2 N_{sx}\bar{\theta}_s^0 u_n,\\
&\tilde{u}_n' = \tilde{\gamma}_n + \mu_n\tilde{v}_n - \bar{\theta}_s^0\mu_n\tilde{w}_n,\\
&\tilde{v}_n' = \tilde{\varepsilon}_n - \frac{\tilde{w}_n}{R} - \bar{\theta}_s^0\tilde{\theta}_n,\\
&\tilde{\bar{N}}_n' = -\mu_n^2 N_s^0\bar{\theta}_s^0\tilde{w}_n - \frac{\tilde{\bar{Q}}_n}{R} + \mu_n^2\left(N_x^0 + N_s^0\right)\tilde{v}_n - \mu_n\tilde{\bar{S}}_n + \mu_n N_s^0\tilde{\gamma}_n -\\
&\qquad - N_{sx}^0\mu_n\left(\varepsilon_n - \bar{\theta}_s^0\theta_n\right) - N_{sx}^0\mu_n^2 u_n,\\
&\tilde{\bar{S}}_n' = \mu_n^2 N_x^0\tilde{u}_n + \mu_n\tilde{N}_{xn} + \mu_n N_{sx}^0\left(\gamma_n - \mu_n v_n + \mu_n\bar{\theta}_s^0 w_n\right),
\end{aligned}
\right\} \qquad (2.30)
$$

Additionally, we introduced $\mu_n = \pi/\ell_n$.

The similar way may be used to transform the equations for rods, the boundary conditions of form (2.23), and compatibility conditions for longitudinal edges of elements in the system.

Substitution of (2.24') into elasticity relations (2.21) allows us to express the variables ε_n, $æ_n$, γ_n, $\tilde{\varepsilon}_n$, $\tilde{æ}_n$, $\tilde{\gamma}_n$, N_{xn}, M_{xn}, H_n, $\tilde{N}_{xn}$, $\tilde{M}_{xn}$, $\tilde{H}_n$ (which are present in (2.30)) in terms of basic variables

$$
\{u\} = \left\lfloor w_n\ \theta_n\ M_n\ \bar{Q}_n\ u_n\ v_n\ \bar{N}_n\ \bar{S}_n\ \tilde{w}_n\ \tilde{\theta}_n\ \tilde{M}_n\ \tilde{\bar{Q}}_n\ \tilde{u}_n\ \tilde{v}_n\ \tilde{\bar{N}}_n\ \tilde{\bar{S}}_n \right\rfloor^T. \qquad (2.31)
$$

For example, values of $\{\varepsilon_n,\ æ_n,\ \tilde{\gamma}_n\}$ and $\{\tilde{\varepsilon}_n,\ \tilde{æ}_n,\ \gamma_n^*\}$ should be determined from the following systems of equations:

$$
\begin{bmatrix} B_{22} + N_s^0 & C_{22} & B_{23} \\ C_{22} & D_{22} & C_{23} \\ B_{32} & C_{32} & B_{33} + N_s^0 \end{bmatrix}
\begin{Bmatrix} \varepsilon_n \\ æ_n \\ \tilde{\gamma}_n \end{Bmatrix} =
\begin{Bmatrix} \bar{N}_n + N_{sx}^0\mu_n\tilde{v}_n + N_s^0\bar{\theta}_s^0\theta_n \\ M_n \\ \tilde{\bar{S}}_n + N_{sx}^0\mu_n u_n - N_s^0\left(\mu_n\tilde{v}_n - \bar{\theta}_s^0\mu_n\tilde{w}_n\right) \end{Bmatrix} +
$$

$$
+ \begin{bmatrix} B_{21}\mu_n & -C_{21}\mu_n^2 & C_{23}\mu_n \\ C_{21}\mu_n & -D_{21}\mu_n^2 & D_{23}\mu_n \\ B_{31}\mu_n & -C_{31}\mu_n^2 & C_{33}\mu_n \end{bmatrix}
\begin{Bmatrix} u_n \\ w_n \\ \tilde{\theta}_n \end{Bmatrix}, \qquad (2.32)
$$

$$\begin{bmatrix} B_{22}+N_s^0 & C_{22} & B_{23} \\ C_{22} & D_{22} & C_{23} \\ B_{32} & C_{32} & B_{33}+N_s^0 \end{bmatrix} \begin{Bmatrix} \tilde{\varepsilon}_n \\ \tilde{æ}_n \\ \gamma_n \end{Bmatrix} = \begin{Bmatrix} \tilde{\bar{N}}_n - N_{sx}^0 \mu_n v_n + N_s^0 \bar{\theta}_s^0 \tilde{\theta}_n \\ M_n \\ \bar{S}_n - N_{sx}^0 \mu_n \tilde{u}_n - N_s^0 \left(-\mu_n v_n + \bar{\theta}_s^0 \mu_n w_n \right) \end{Bmatrix} -$$

$$- \begin{bmatrix} B_{21}\mu_n & C_{21}\mu_n^2 & C_{23}\mu_n \\ C_{21}\mu_n & D_{21}\mu_n^2 & D_{23}\mu_n \\ B_{31}\mu_n & C_{31}\mu_n^2 & C_{33}\mu_n \end{bmatrix} \begin{Bmatrix} \tilde{u}_n \\ \tilde{w}_n \\ \theta_n \end{Bmatrix}, \qquad (2.33)$$

and, similarly, the stress resultants and moments $\{N_{xn}, M_{xn}, \tilde{H}_n\}$ and $\{\tilde{N}_{xn}, \tilde{M}_{xn}, H_n\}$ would be found from the equations,

$$\begin{Bmatrix} N_{xn} \\ M_{xn} \\ \tilde{H}_n \end{Bmatrix} = \begin{bmatrix} -B_{11}\mu_n & C_{11}\mu_n^2 & -C_{13}\mu_n \\ -C_{11}\mu_n & D_{11}\mu_n^2 & -D_{13}\mu_n \\ -C_{31}\mu_n & D_{31}\mu_n^2 & -2D_{33}\mu_n \end{bmatrix} \begin{Bmatrix} u_n \\ w_n \\ \tilde{\theta}_n \end{Bmatrix} + \begin{bmatrix} B_{12} & C_{12} & B_{13} \\ C_{12} & D_{12} & C_{13} \\ C_{32} & D_{32} & C_{33} \end{bmatrix} \begin{Bmatrix} \varepsilon_n \\ æ_n \\ \tilde{\gamma}_n \end{Bmatrix}, \qquad (2.34)$$

$$\begin{Bmatrix} \tilde{N}_{xn} \\ \tilde{M}_{xn} \\ H_n \end{Bmatrix} = \begin{bmatrix} B_{11}\mu_n & C_{11}\mu_n^2 & C_{13}\mu_n \\ C_{11}\mu_n & D_{11}\mu_n^2 & D_{13}\mu_n \\ C_{31}\mu_n & D_{31}\mu_n^2 & 2D_{33}\mu_n \end{bmatrix} \begin{Bmatrix} \tilde{u}_n \\ \tilde{w}_n \\ \theta_n \end{Bmatrix} + \begin{bmatrix} B_{12} & C_{12} & B_{13} \\ C_{12} & D_{12} & C_{13} \\ C_{32} & D_{32} & C_{33} \end{bmatrix} \begin{Bmatrix} \tilde{\varepsilon}_n \\ \tilde{æ}_n \\ \gamma_n \end{Bmatrix}. \qquad (2.35)$$

The relevant matrix-based problem statement and the solution method completely coincide with those proposed above; however, dimensions of all vectors and matrices are twice as much, so in the general case

$$\{y_i\} = \left\lfloor w_{ni}\ \theta_{ni}\ u_{ni}\ v_{ni}\ \tilde{w}_{ni}\ \tilde{\theta}_{ni}\ \tilde{u}_{ni}\ \tilde{v}_{ni} \right\rfloor^T, \quad i = 1,2,\ldots,N.$$

Integral stiffnesses B_{ij}, C_{ij}, and D_{ij} of multilayered composite element should be evaluated on the basis of elastic properties of layers present in the stack; use is made of the methods exposed in [11, 12]; if early buckling takes place, these are replaced with tangential characteristics considered in Section 2.1. Any component in the system can be isotropic, metallic or orthotropic "by design" (refer to [10]).

This means that the method for numerically analyzing built-up cylindrical structures that had been developed by the authors in [13] is now made capable to deal with structures which incorporate composite materials.

The present method and the respective software programs can be employed to solve many classical problems (for which the researchers have provided exact and/or reliable approximate solutions), new problems of structural buckling, as well as complicated problems on stability of built-up composite structures that appear in designer's practical work.

For example, Table 1 compares the new numerically obtained results with the exact solution of [12] for a rectangular orthotropic plate simply supported at all four edges. Analyses were performed assuming the following parameters:

— the total number of orthogonalization points for each element, $n_0 = 10$,

— the total number of Runge-Kutta steps between orthogonalization points, $n_{P-K} = 10$,

— the allowable relative error in the t_n determination procedure, $\varepsilon = 0.001$.

Table 1

$$k = \overline{N}_{x*} = \left(\frac{N_x b^2}{\pi^2 \sqrt{D_1 D_2}} \right)_*$$

$\varepsilon = 10^{-3}$
$n_0 = 10$
$n_{P-K} = 10$

a/b	$D_1 = d_{11}$	$D_2 = d_{22}$	$D_3 = d_{12} + 2d_{33}$	b	n*	k	
						Exact solution	Numerical solution
1	10^4	$16D_1$	D_1	200π	2	2.5	2.5011
8	$16D_2$	10^4	D_2	200π	4	2.5	2.5011
1	$16D_2$	10^4	D_2	200π	1	4.75	4.7523
1	$4 \cdot 10^4$	D_1	D_1	200π	1	4.0	4.0006

It is clearly seen that the error of the numerical solution at the aforementioned procedural parameters does not exceed 0.05% and the critical load thus obtained is above the exact value.

A similar result is seen in comparison of the exact value of stability coefficient, k=7.69 (refer to [14]) and the numerically obtained one, k=7.6916, for the problem of buckling of a square isotropic plate with clamped longitudinal edges.

As for the boundary condition version mentioned, we find it interesting to estimate the accuracy of the work [15] simplified solution which is widely used in analysis of composite plates. The solution is compared with the newly obtained data in Table 2 and shown to overestimate the critical load by 1.6% to 4%.

Table 2

$$k = \overline{N}_{x*} = \left(\frac{N_x b^2}{\pi^2 \sqrt{D_1 D_2}} \right)_*$$

$\varepsilon = 10^{-3}$
$n_0 = 10$
$n_{P-K} = 10$

a/b	$D_1 = d_{11}$	$D_2 = d_{22}$	$D_3 = d_{12} + 2d_{33}$	b	n*	k	
						Exact solution	Numerical solution
1	$4 \cdot 10^4$	D_1	D_1	200π	2	8	7.6916
1	$16D_2$	10^4	D_2	200π	1	6	5.9022
8	$16D_2$	10^4	D_2	200π	6	5.28	5.1562

Further, we solved the problem on stability of a longitudinally compressed composite panel whose stiffeners are longitudinal webs with a rectangular cross section. Panel dimensions are a=500 mm and b=300 mm; stiffener spacing is 60 mm; stiffener thickness x height, 3.64 mm x 30 mm; and skin thickness, 2.34 mm. A stiffener has a stacking sequence $[+45_2/-45_2/0_{10}]_s$, and the skin, $[+45_2/-45_2/0_4/90]_s$; ply characteristics are E_1=20930 kg/sq.mm, E_2=800 kg/sq.mm, G_{12}=520 kg/sq.mm, $\nu_{12}=0.26$, $\delta=0.13$ mm.

Consideration was given to

— global buckling (Fig. 2.9a) for the panel with unsupported longitudinal edges and

— local buckling (Fig. 2.9b) for the panel with simply supported longitudinal edges.

In the case of global buckling the panel has one half-wave ($n_*=1$) and the critical compressive load $P_*=57500$ kg; and in the case of local buckling, $n_*=5$, $\ell_*=a/n_*=100$ mm, and $P_*=92500$ kg.

Also, we treated the problem on buckling of a shear-loaded long composite plate (a=2000 mm, b=500 mm) whose layers have E_1=27000 kg/sq.mm, E_2=2000 kg/sq.mm, G_{12}=980 kg/sq.mm, ν_{12}=0.22, δ_{ply}=0.1 mm. The stacking sequence was defined as $[0/90/\alpha_4]_s$ where the angle α was varied from 0 to +90 and from 0 to -90.

Figure 2.10 represents the dependence of the critical shear load N_{sx} on the angle α of the eight middle layers. One can see that if the angle α is negative, the critical shear load is maximum at the angle of approximately -60°. If the angle α is positive, the critical shear load is much lower.

Figure 2.11 demonstrates how the critical compressive load N_x of the same plate depends on the angle α of the eight middle layers. The critical load is maximum at α=45°.

Of particular interest is stability of a composite plate in which certain layers are disbonded over a domain with the length ξ. Even if the initial layup was symmetric, the debonding makes the panel become a structure with two asymmetric stacks over the domain mentioned. This system may well be analyzed by the above methods and software programs since these are capable to treat the structure as a system of asymmetric elements included in the general model.

Used as an example may be the problem for a composite panel with the stacking sequence $[90/0/+45_2/-45_2/90_4/0]_s$. Each ply is assumed to have the following characteristics: E_1=18000 kg/sq.mm, E_2=900 kg/sq.mm, G_{12}=514 kg/sq.mm, ν_{12}=0.31, δ_{ply}=0.05 mm. Panel sizes are a=120 mm and b=40 mm. Now we presume that three upper layers at the center of the plate are not bonded over the length ξ which is varied in the course of the analyses.

Theoretical results are shown in Fig. 2.12 together with the analytical model comprising five elements and five nodes. Elements 2, 3, and 4 feature an asymmetric layup and anisotropy.

In the debonding domain the subcritical stress resultant is distributed between the upper and lower stacks in accordance with the deformation compatibility condition for the limiting points of the debonding domain.

Dependence of the critical load N_s on the relative debonding domain length ξ/b is shown in Fig. 2.12 by the solid line. The dashed line represents the critical load for an intact plate, and the dash-and-dot line corresponds to the critical load for a stepwise plate with disbonded layers removed in the domain with the length ξ.

Analyzing the solid line in Fig. 2.12, it is clear that a short debonding domain ($\xi/b \le 0.1$) does not cause the substacks to separate, so the plate is buckling as a whole following the usual global buckling shape. One can see an insignificant decrease in the critical load for the interval $\{0 \le \xi/b \le 0.1\}$; the reason is the stack stiffness being reduced in the debonding domain.

If $\xi/b > 0.1$ the thin part of the plate is buckling, with the rest of the plate being almost straight and capable of carrying a load increment. At higher loads the stiffness of the thin part gets reduced, which is followed by global buckling; the critical load at the moment of reaching the load-carrying capacity limit corresponds to the critical load for a panel with a weakened part over the disbonded area.

CONCLUSION

In compliance with the NCCW-1-233 the investigation into the influence of the skin postbuckling load-bearing capability on general stress and strains and on stability of composite structures has been accomplished.

The following results have been generated:

— a simplified method for analyzing stresses and strains and load redistribution between structural components which is caused by skin buckling;

— a nonlinear finite element method taking into account the skin postbuckling load-bearing capability;

— an analytical solution to stability problems; evaluation of the effect of the skin postbuckling behavior on general stability of stiffened composite panels and shells;

— a high-accuracy numerical method for analyzing stability of built-up cylindrical structures that allows for discrete stiffening, nonuniform multiaxial load, and skin postbuckling behavior.

The results and proposals on further research work would be discussed with NASA experts.

REFERENCES

1. Zamula G.N., Kut'inov V.F., Vasil'yev V.V., Grishin V.I., Ierusalimsky K.M., Azikov N.S., Begeev T.K. Composite panel postbuckling behavior and general model of joints in composite structures, Moscow, TsAGI-MATI, 1996.

2. Zamula G.N., Vasil'yev V.V., Kut'inov V.F., Grishin V.I., Begeev T.K., Sukhobokova G.P. Analyzing the postbuckling behavior of composite panels and strength of joints in composite structures taking into account temperature effects, Moscow, TsAGI, 1997.

3. Zamula G.N. Numerical analysis of a thin-walled structure with a buckled skin, WCCM-II, Stuttgart, 1990.

4. Zamula G.N., Ierusalimsky K.M. Stability of complex cylindrical structures, Euromech, München, 1991.

5. Birger I.A. Circular plates and shells of revolution. - Oborongiz, Moscow, 1961.

9. Ierusalimsky K.M. On stability of cylindrical shell subjected to torsion and combined load with torsion. - Uchenyye Zapiski TsAGI, 1982, vol. 13, no. 2.

10. Godunov S.K. On numerical solution of boundary-value problems for systems of linear ordinary differential equations. - Uspekhi Matematicheskikh Nauk, 1961, vol. 16, no. 3.

11. Alfutov N.A., Zinov'yev P.A., Popov B.G. Analysis of multilayered composite plates and shells. - Mashinostroyeniye, Moscow, 1984.

12. Lekhnitsky S.G. Anisotropic plates. - Gostekhizdat, Moscow, Leningrad, 1947.

13. Zamula G.N., Ierusalimsky K.M. Stability and thermal stability of cylindrical structures. - Uchenyye Zapiski TsAGI, 1987, vol. 18, no. 6.

14. Vol'mir A.S. Stability of elastic systems. - Fizmatgiz, Moscow, 1963.

15. Composites Handbook, volume 2. - Mashinostroyeniye, Moscow, 1988.

FIGURES

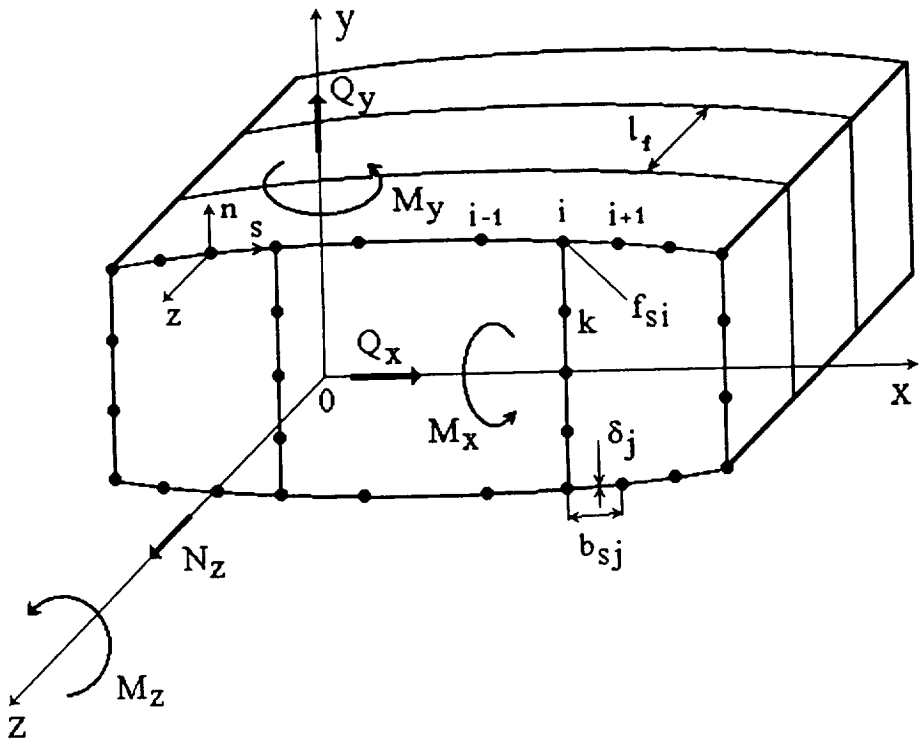

Figure 1.1. A cylindrical section in a stiffened structure

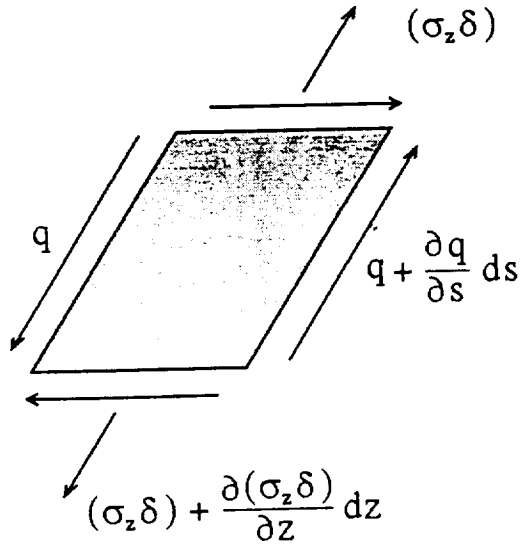

Figure 1.2. Skin cell and its edge stress resultants

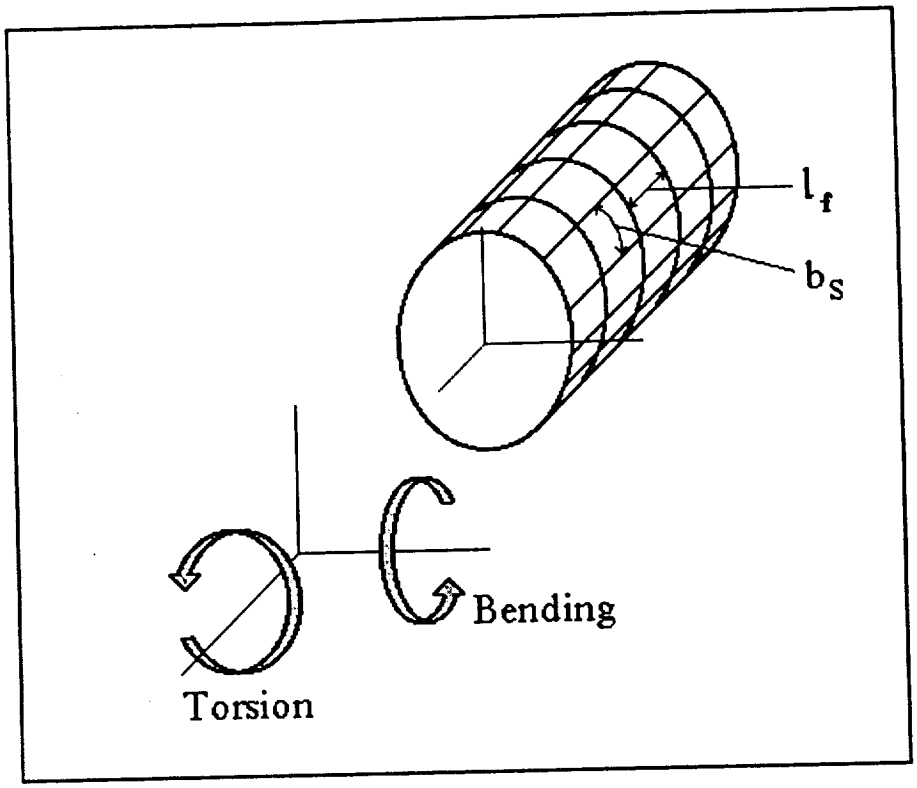

Figure 1.3. A circular section

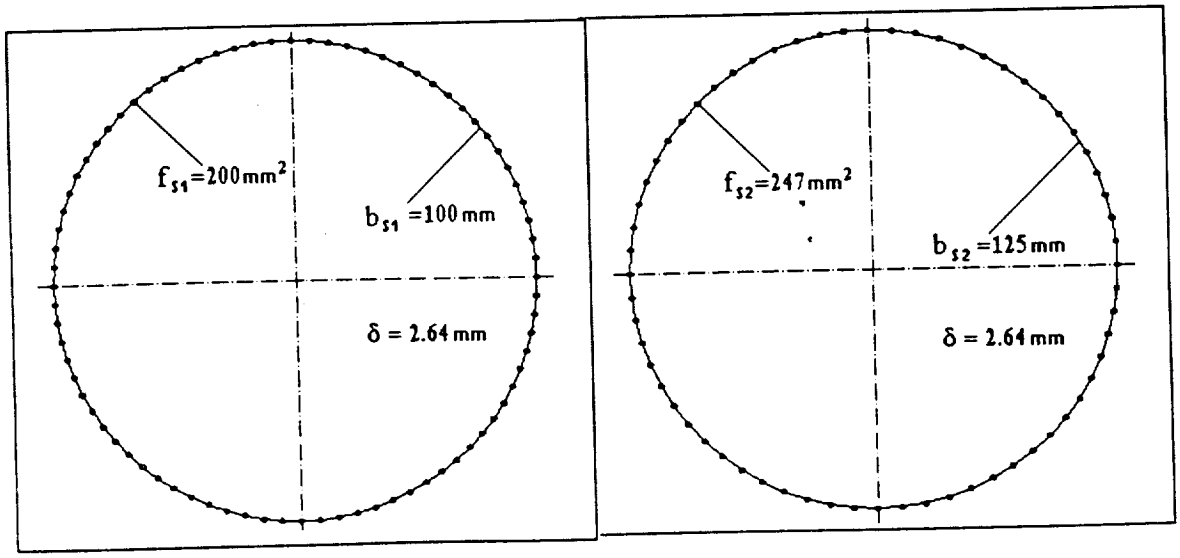

Figure 1.4. Section stiffening

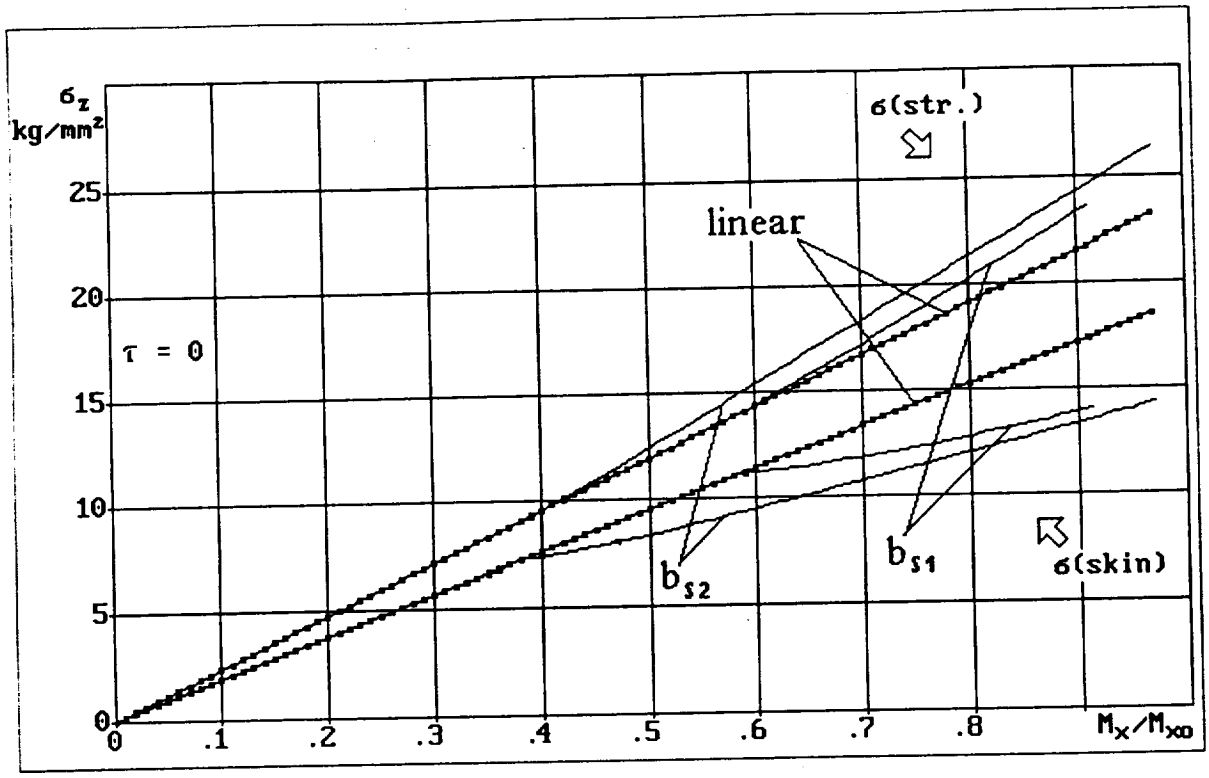

Figure 1.5. Mean stresses in lower panel skin and stiffeners: load A

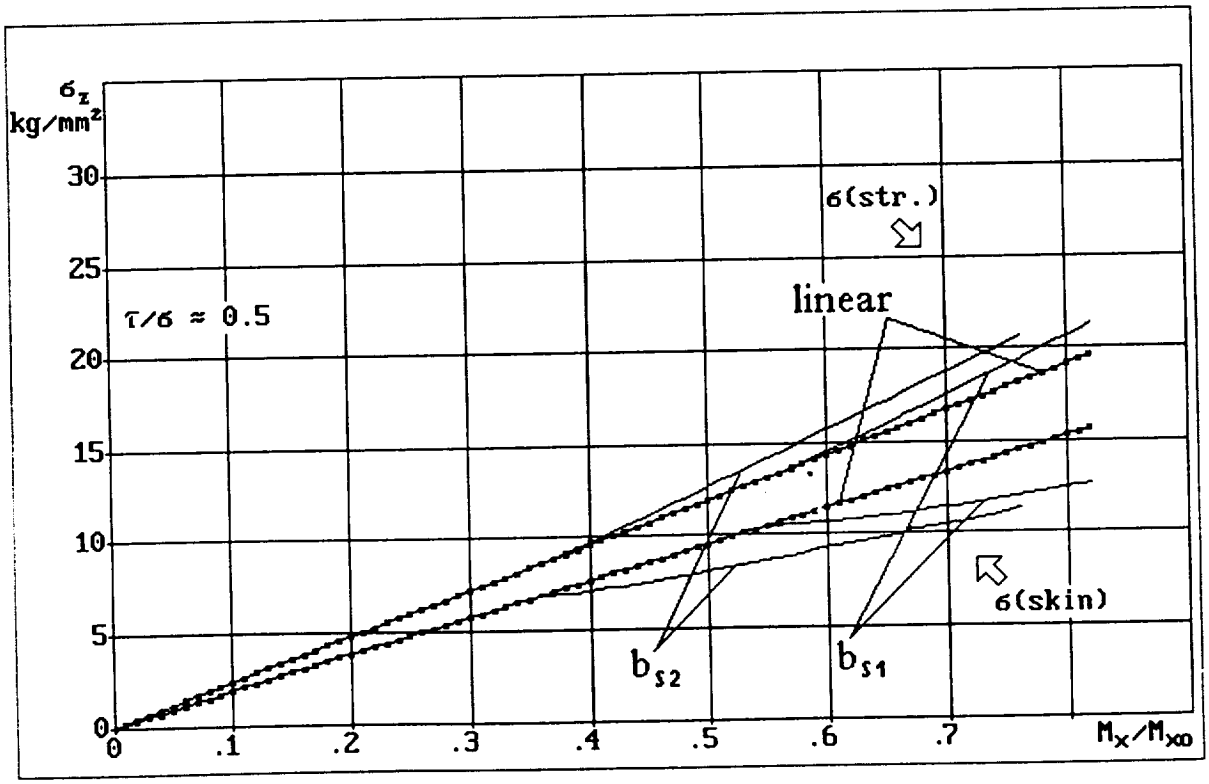

Figure 1.6. Mean stresses in lower panel skin and stiffeners: load B

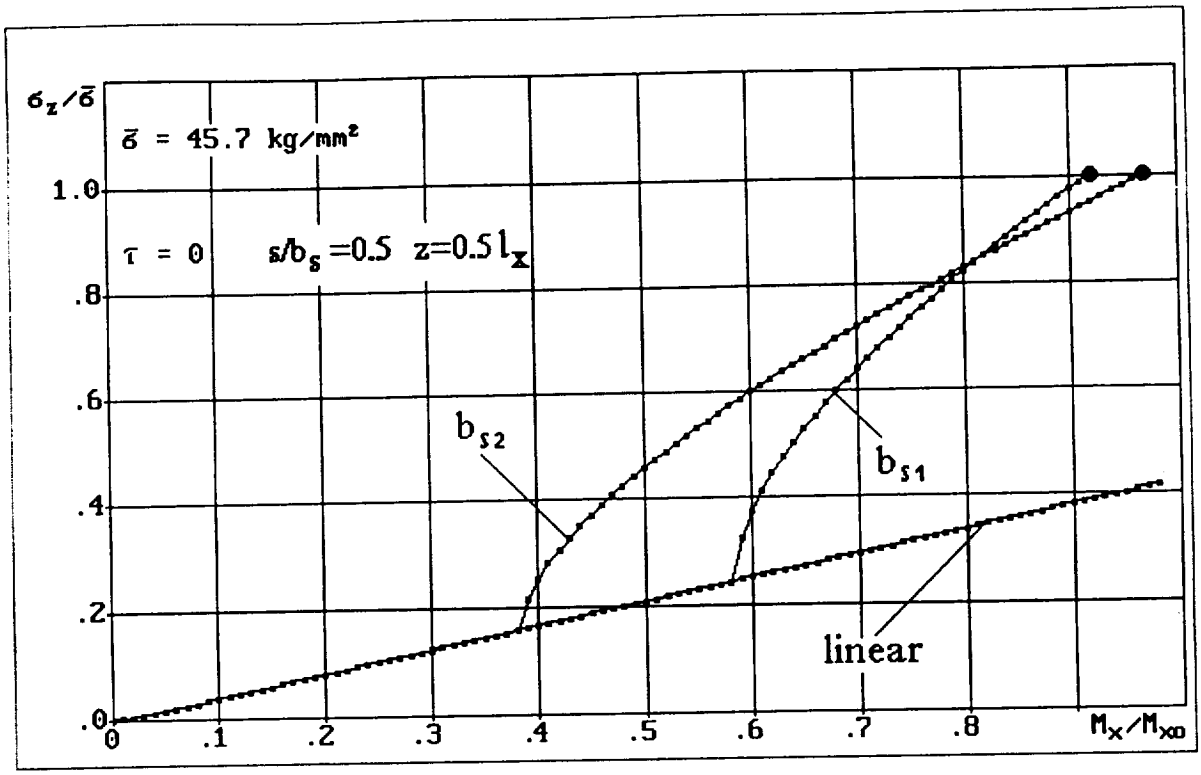

Figure 1.7. Maximum stresses in lower panel skin: load A

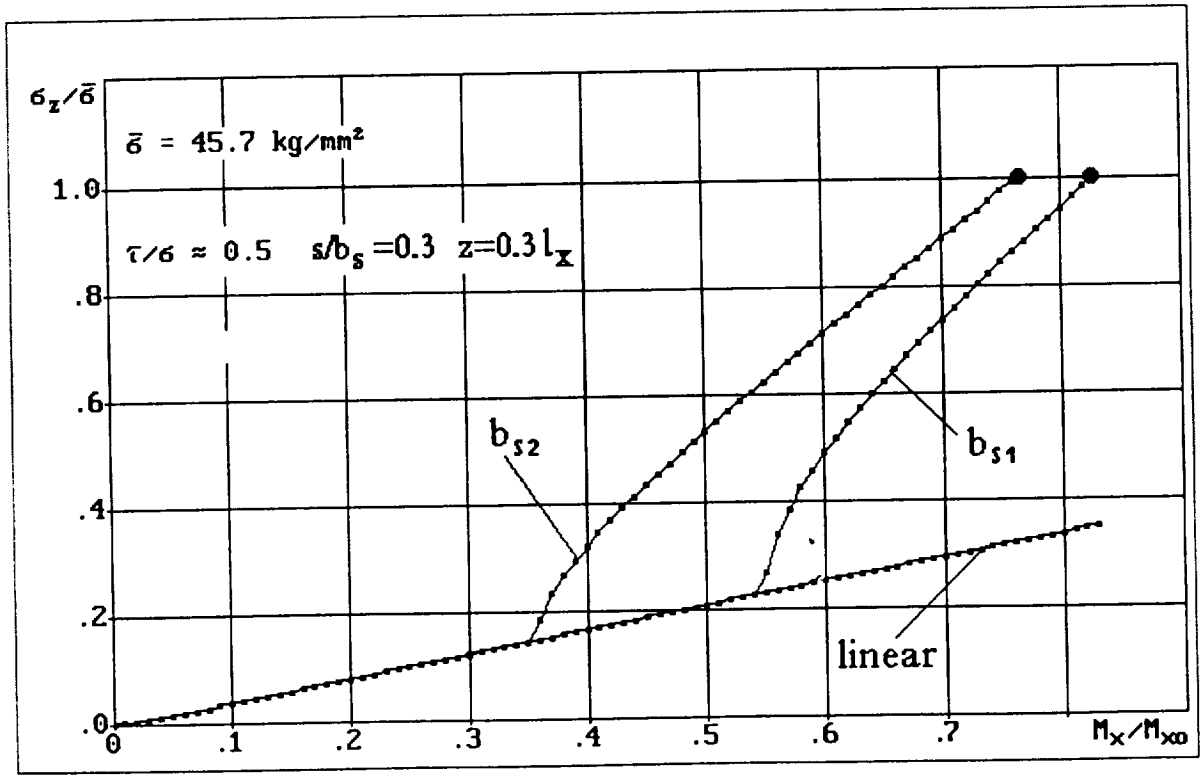

Figure 1.8. Maximum stresses in lower panel skin: load B

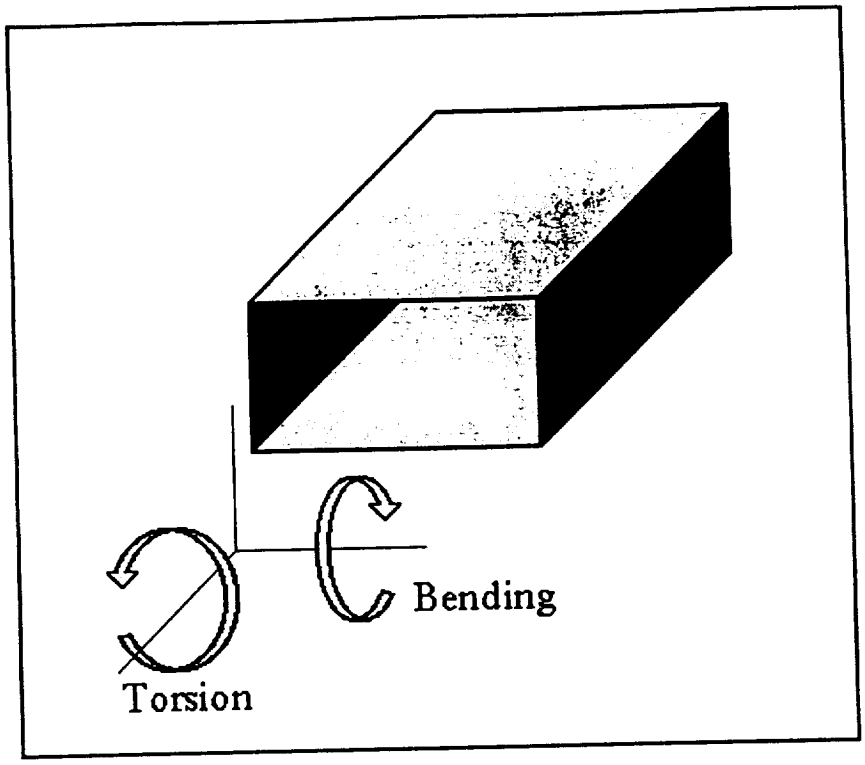

Figure 1.9. Rectangular torsion box

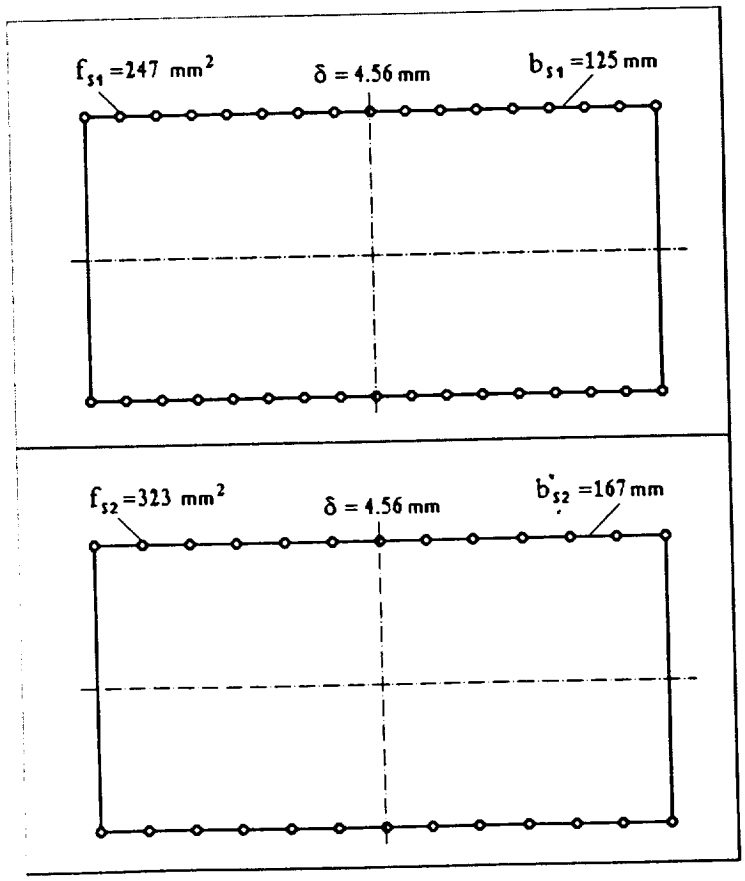

Figure 1.10. Torsion box attachment model

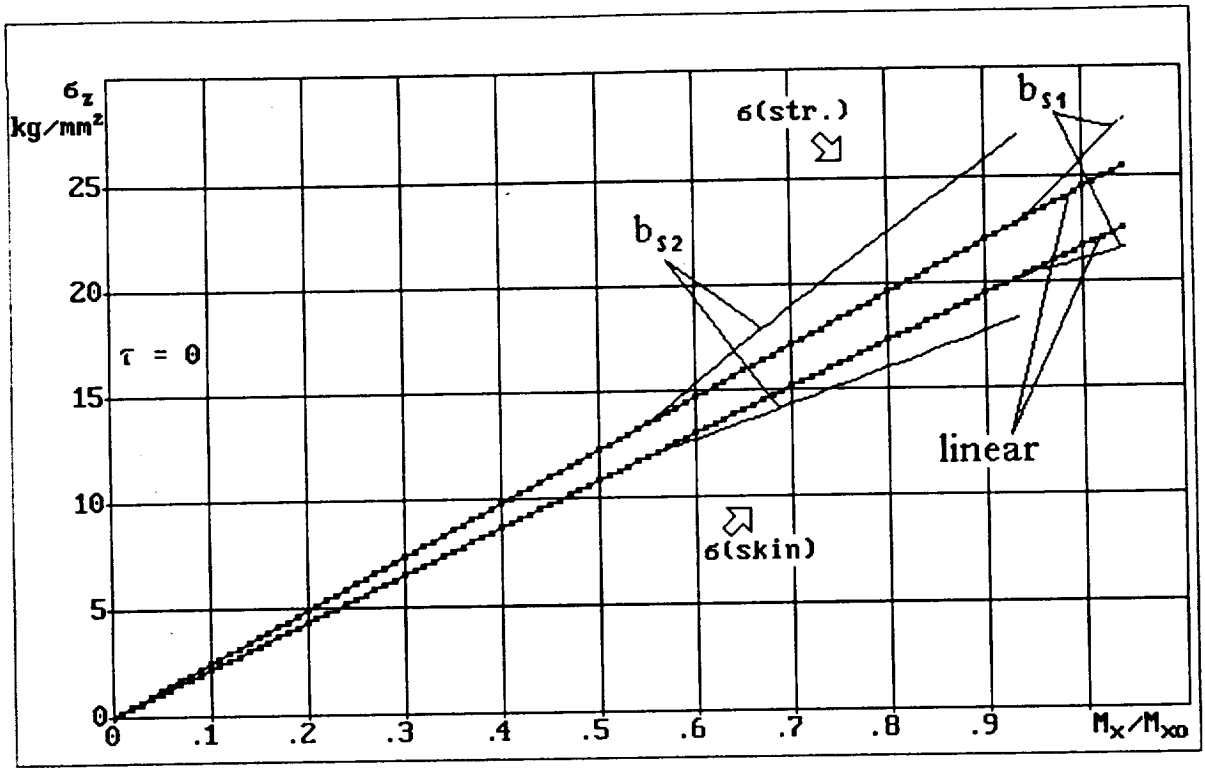

Figure 1.11. Mean stresses in compression-loaded panel skin and stiffeners: load A

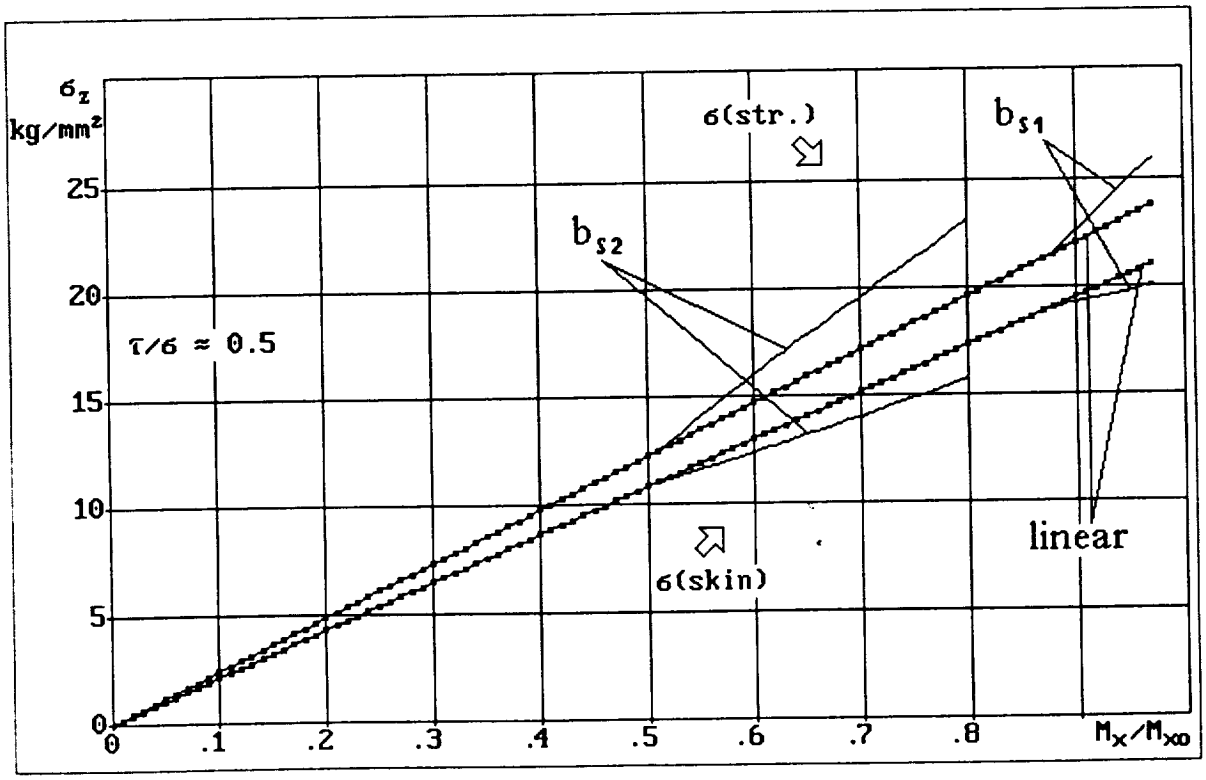

Figure 1.12. Mean stresses in compression-loaded panel skin and stiffeners: load B

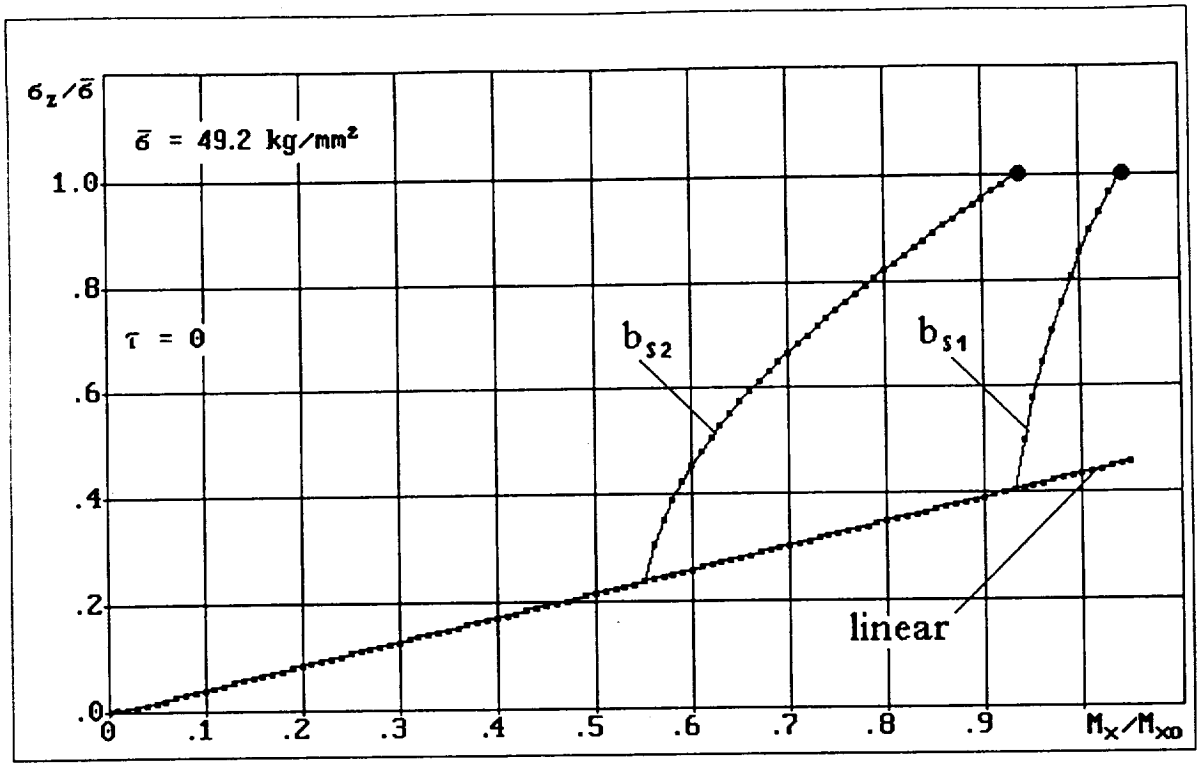

Figure 1.13. Maximum stresses in compression-loaded panel skin: load A

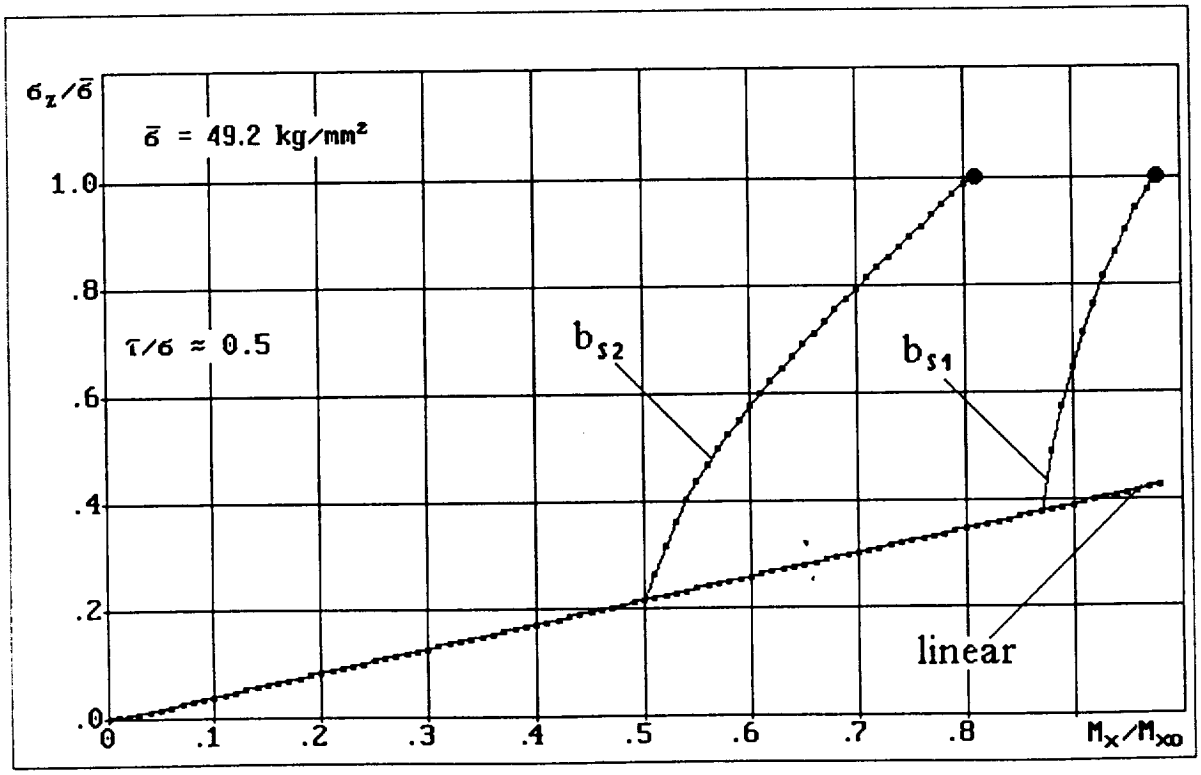

Figure 1.14. Maximum stresses in compression-loaded panel skin: load B

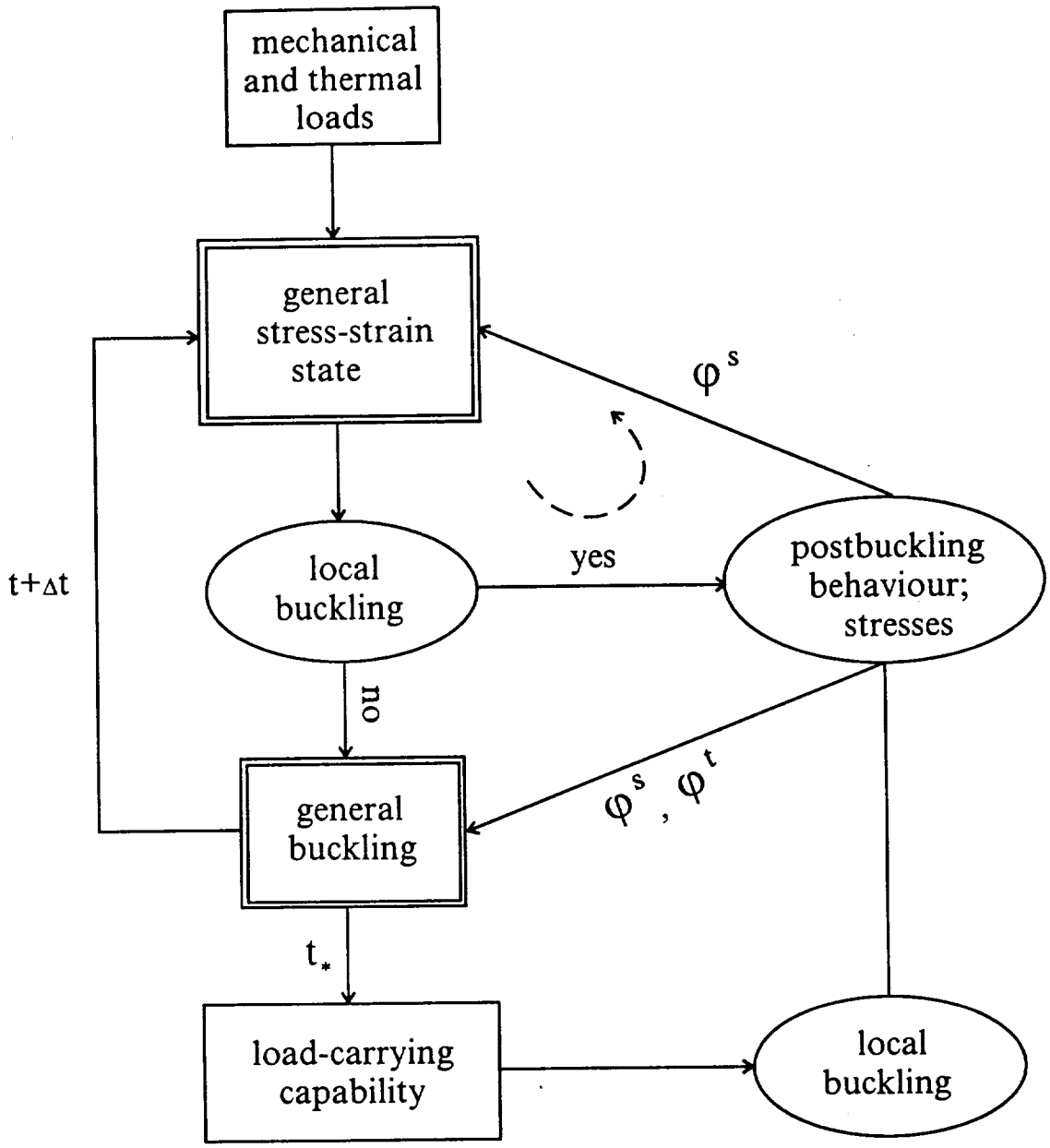
mechanical and thermal loads
general stress-strain state
φ^s
local buckling
yes
postbuckling behaviour; stresses
t+Δt
no
general buckling
φ^s, φ^t
t_*
load-carrying capability
local buckling

Figure 1.15.

Rods in tension/compression

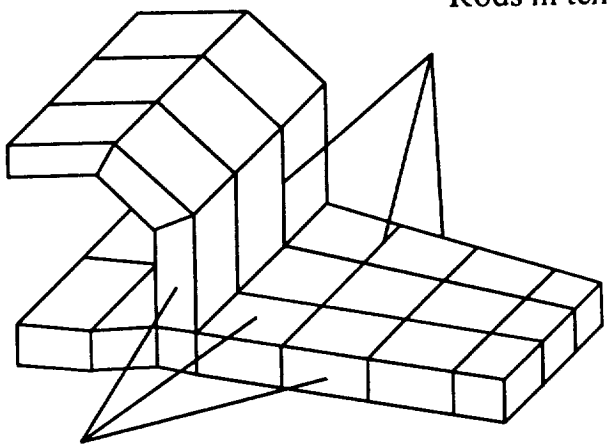

Plates in plane stress

a)

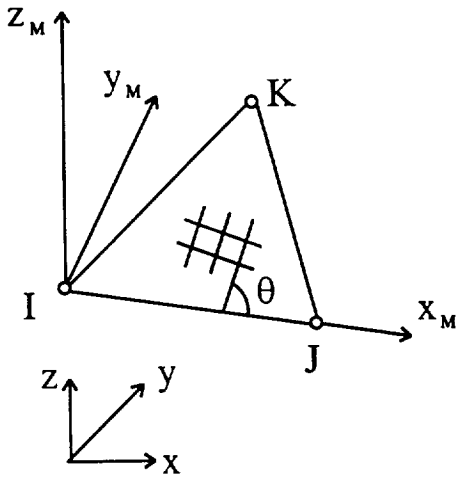

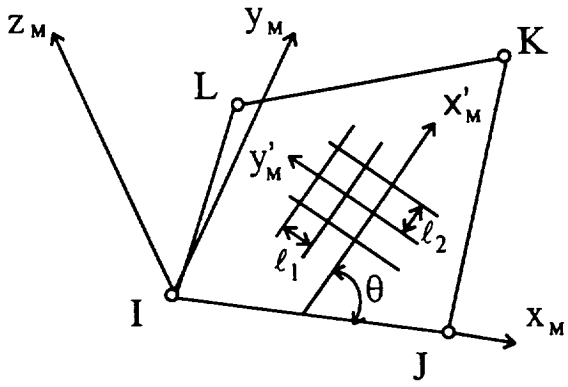

b)

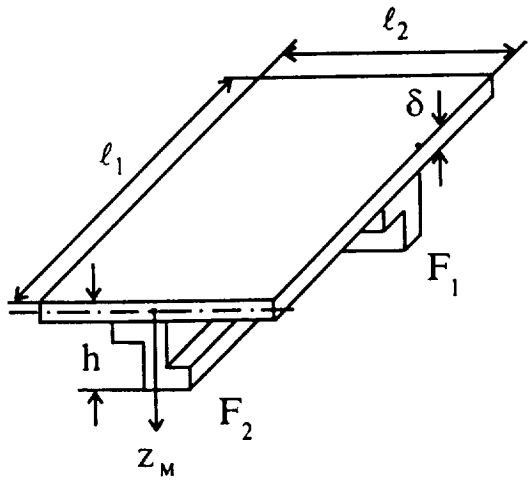

c)

Figure 1.16. Finite element model, finite elements, and part of stiffeners

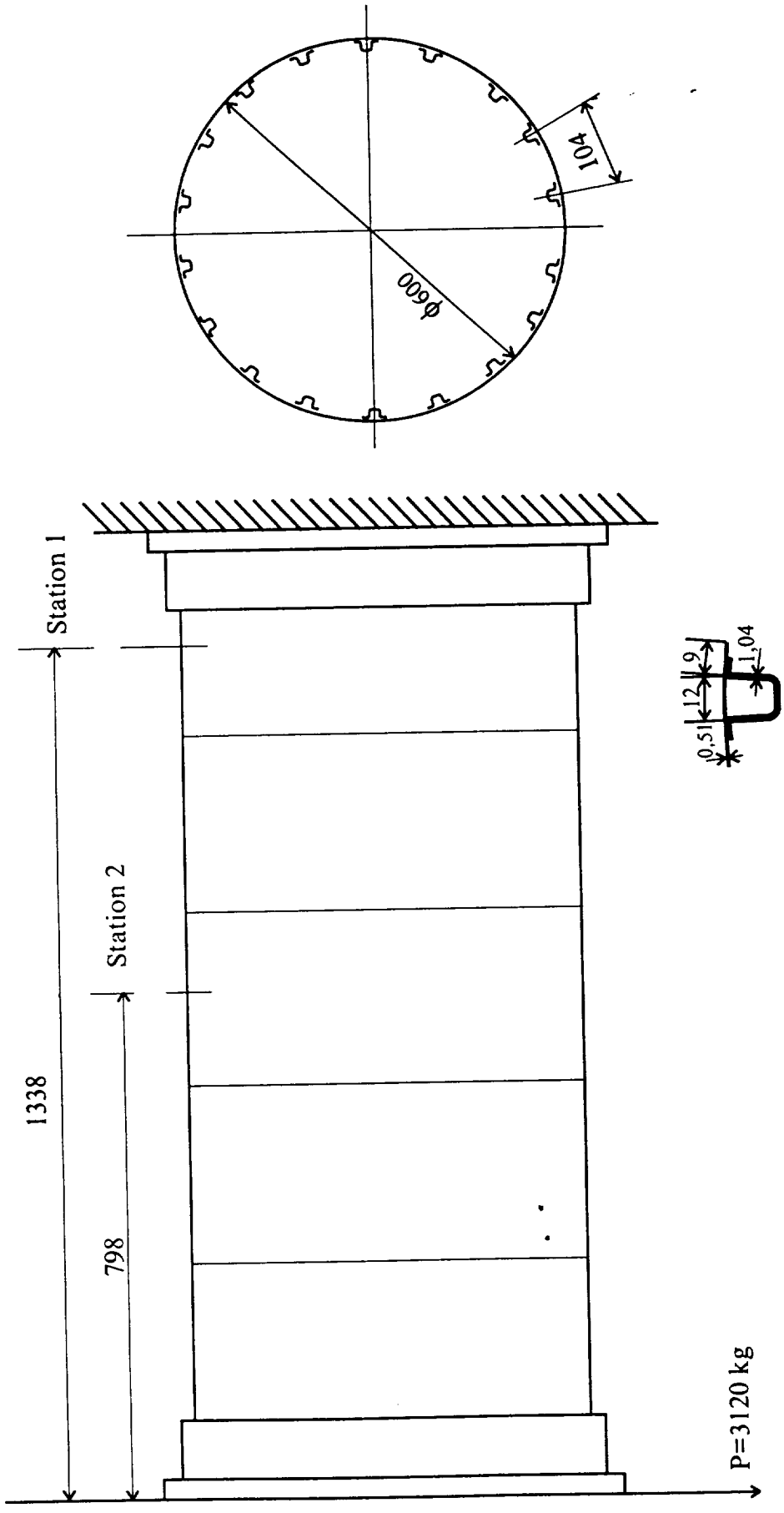

Figure 1.17. Stiffened cylindrical shell loaded with bending

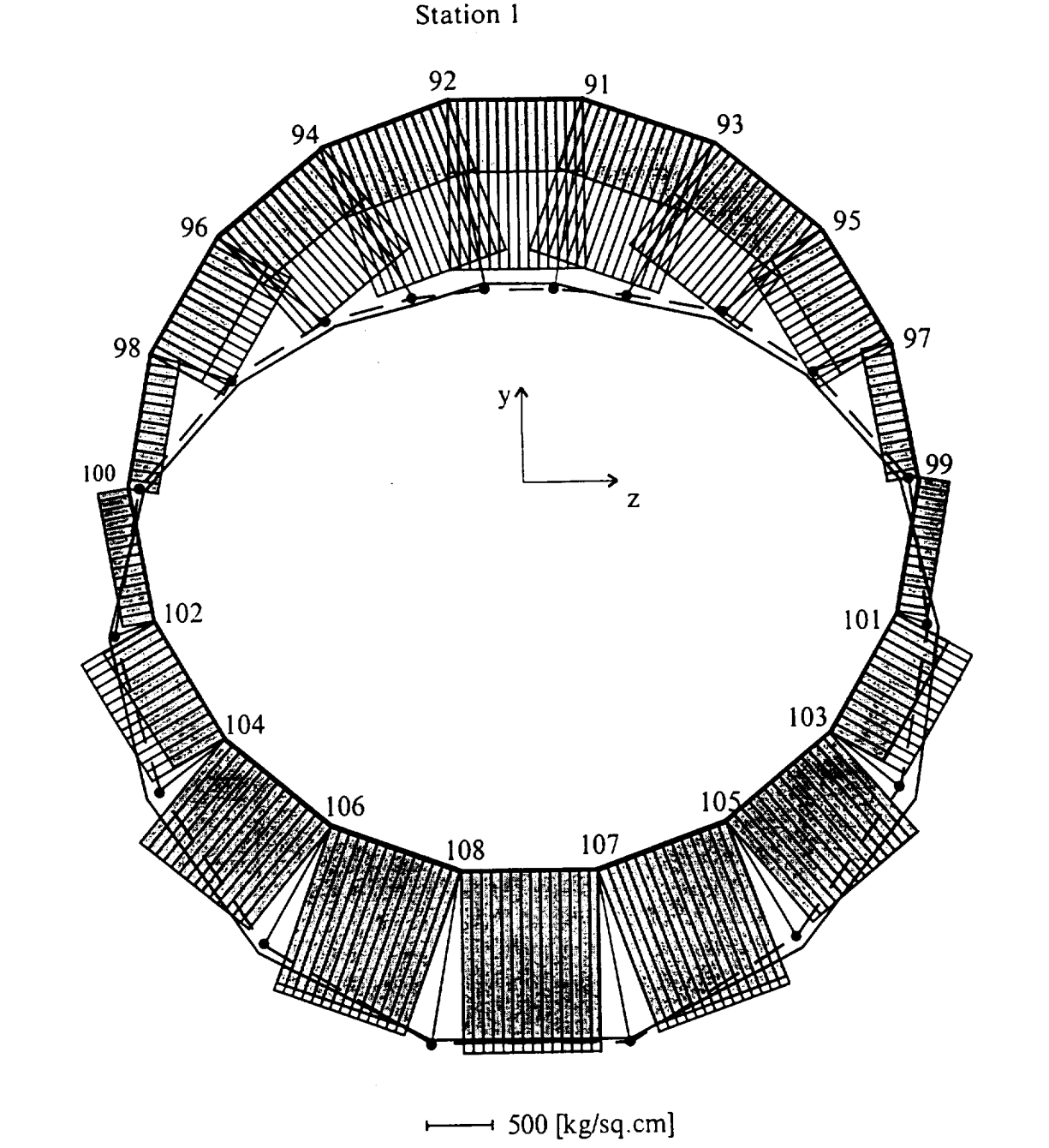

Figure 1.18. Normal stress diagram

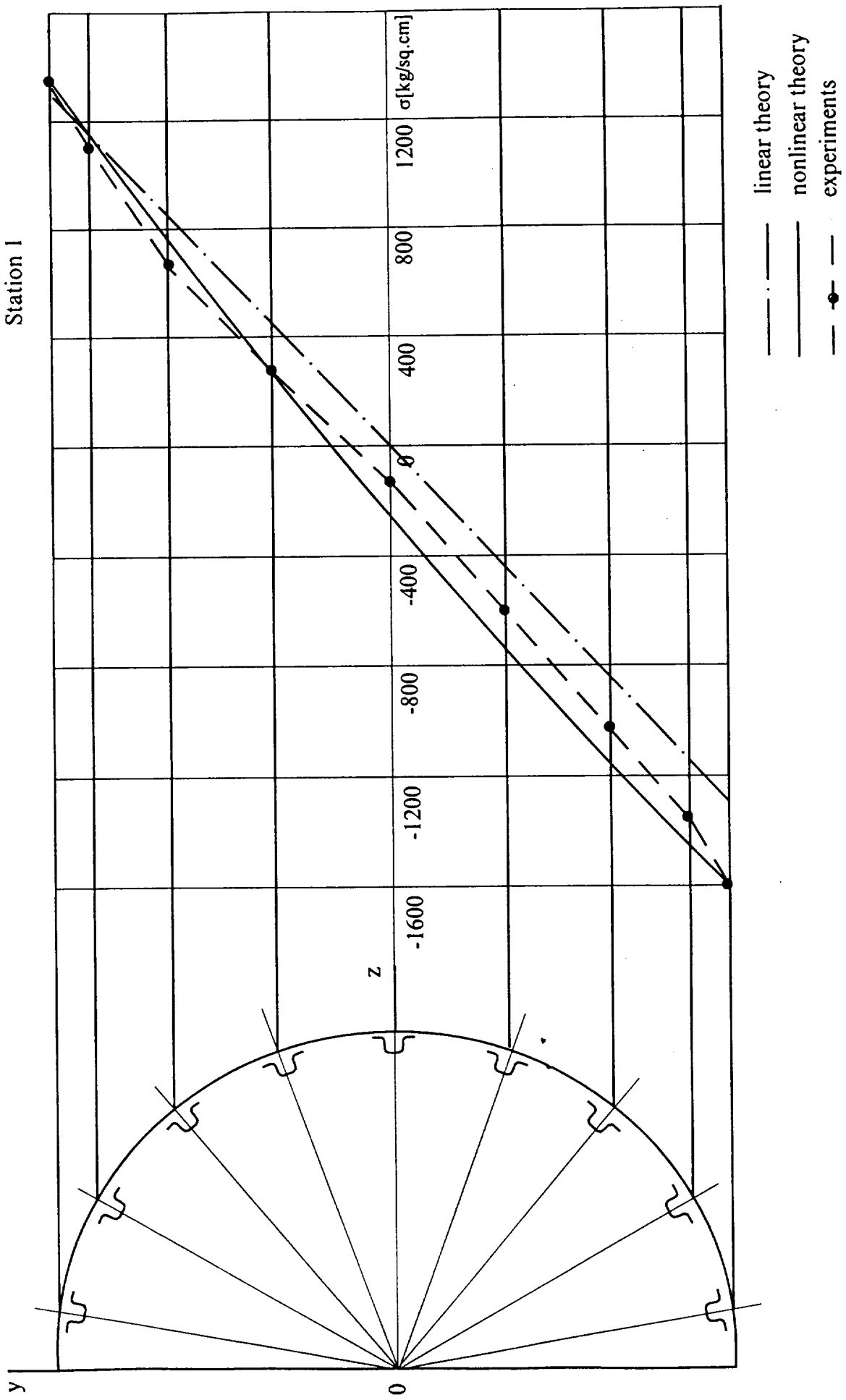

Figure 1.19. Normal stress in stiffeners at clamped end

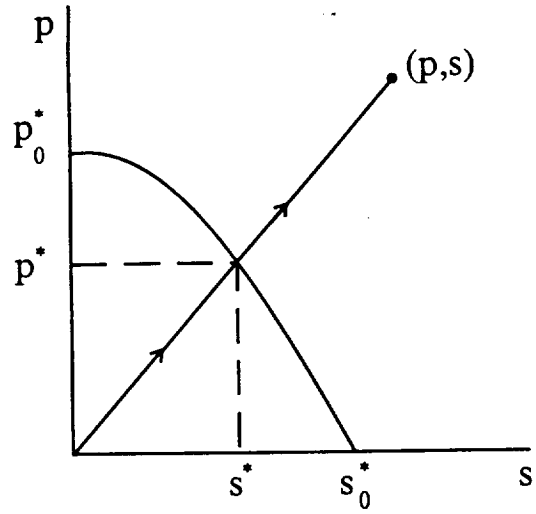

Figure 2.1 The buckling limit and the proportional loading

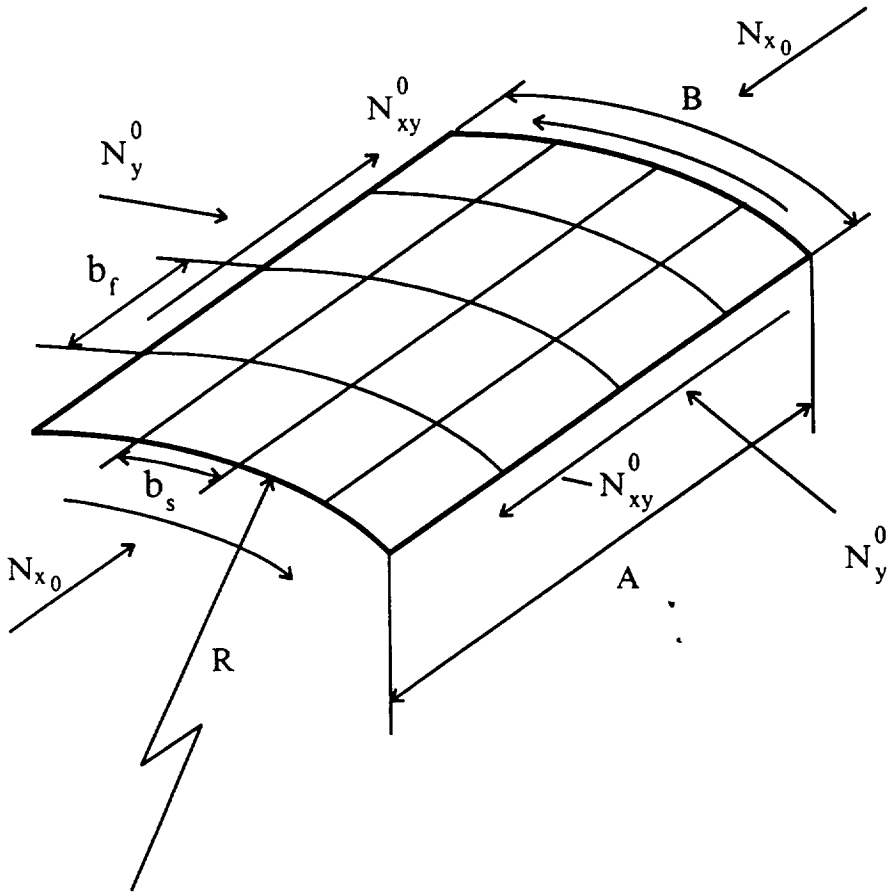

Figure 2.2. Stiffened cylindrical panel

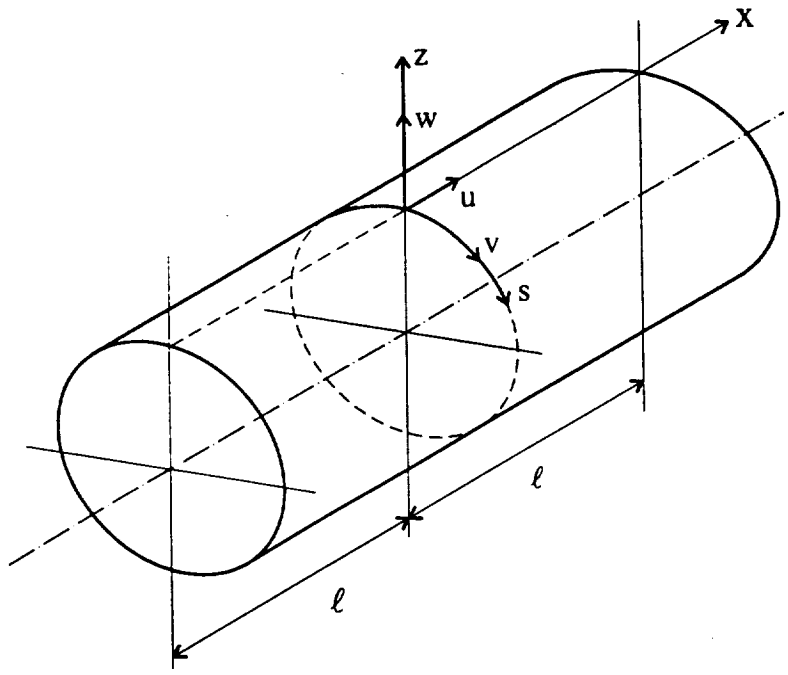

Figure 2.3. Cylindrical shell

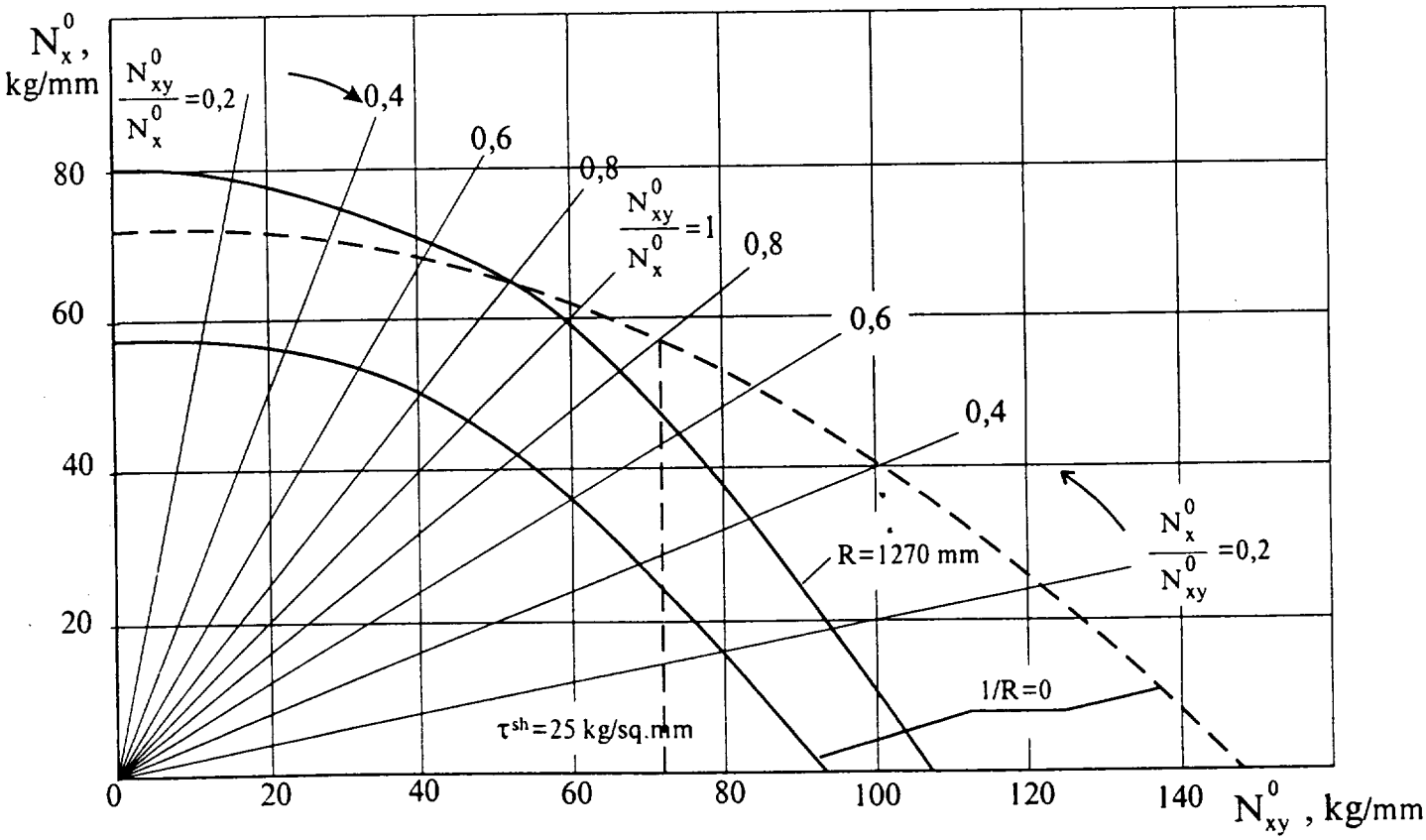

Figure 2.4. The general buckling limit for flat and cylindrical panels

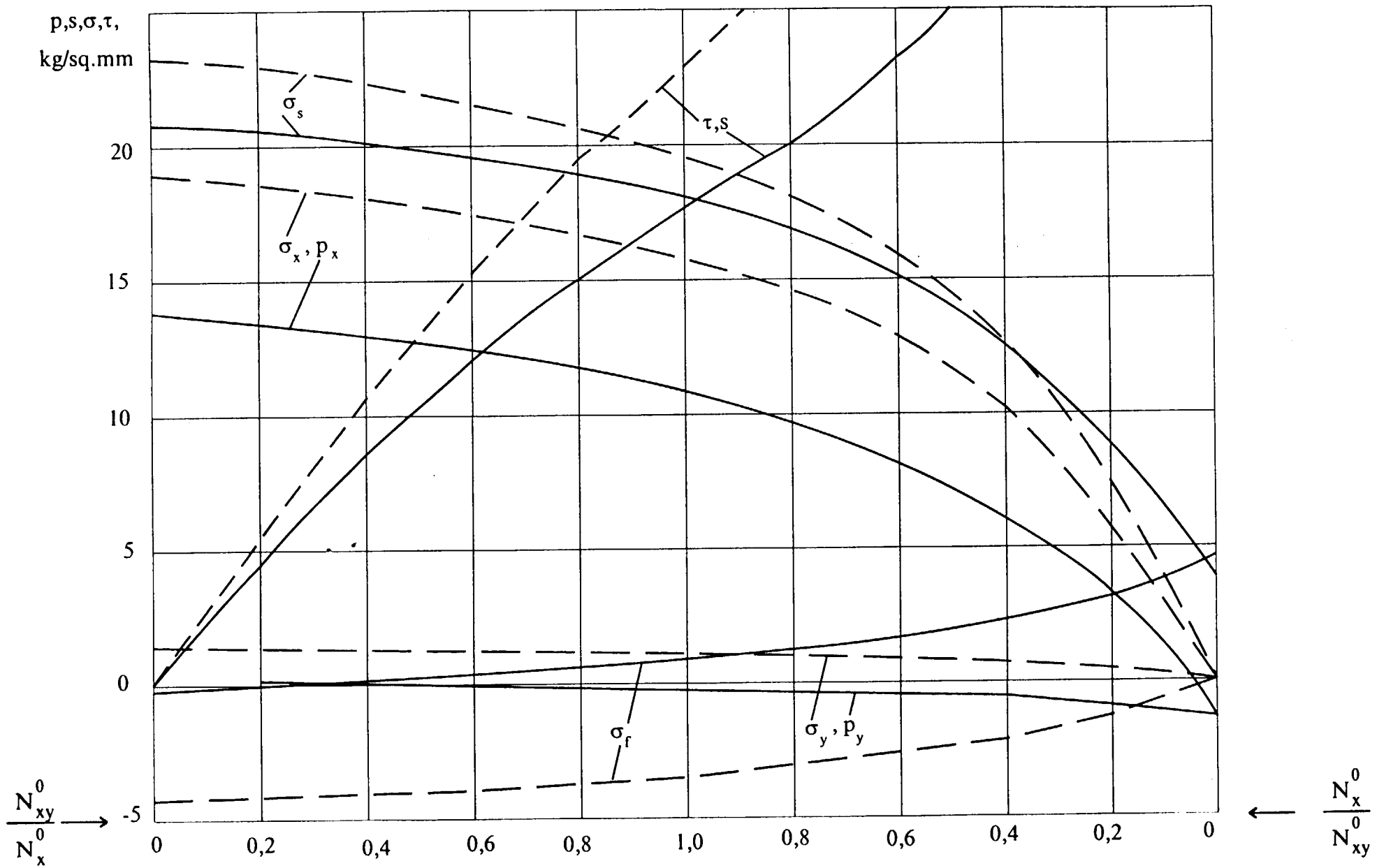

Figure 2.5. Subcritical stresses in panel components

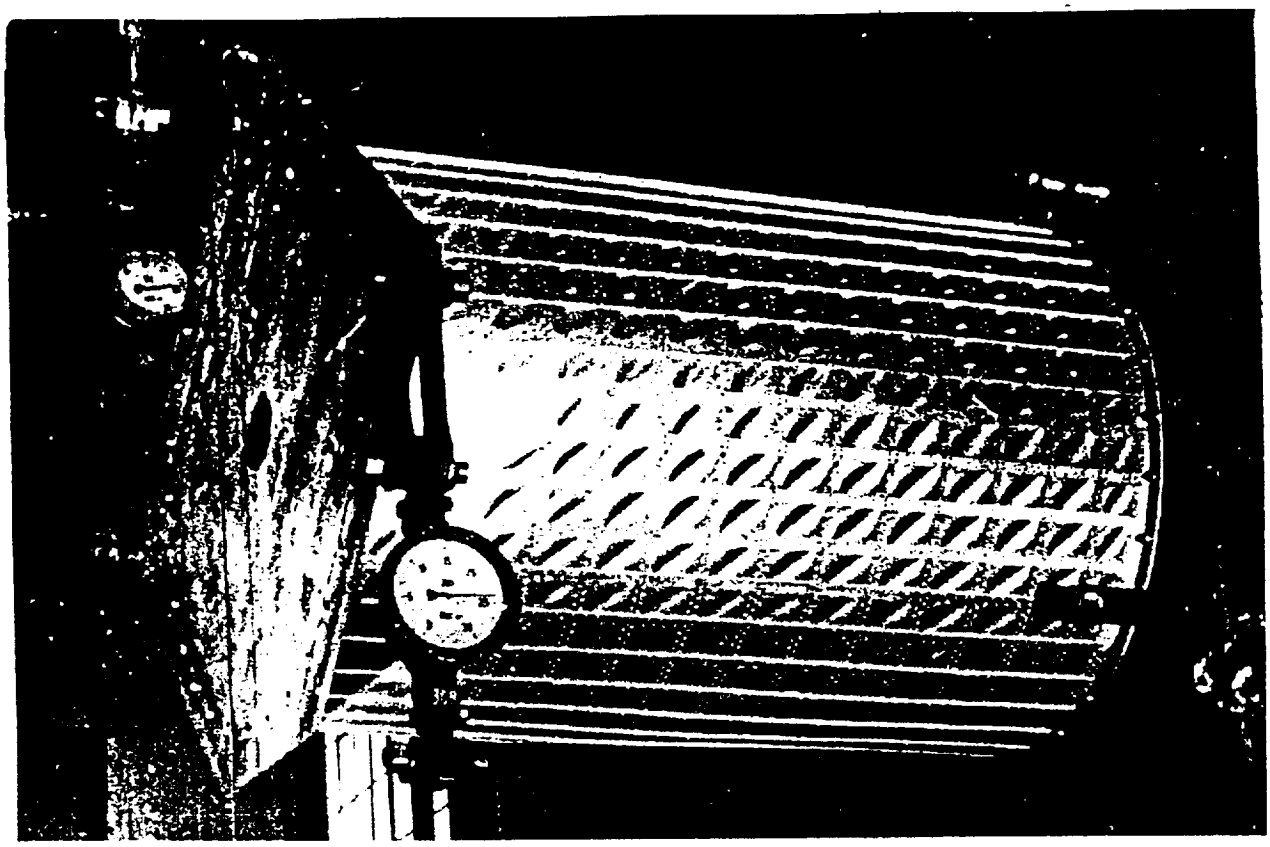

Figure 2.6. Cylindrical shell in subcritical state

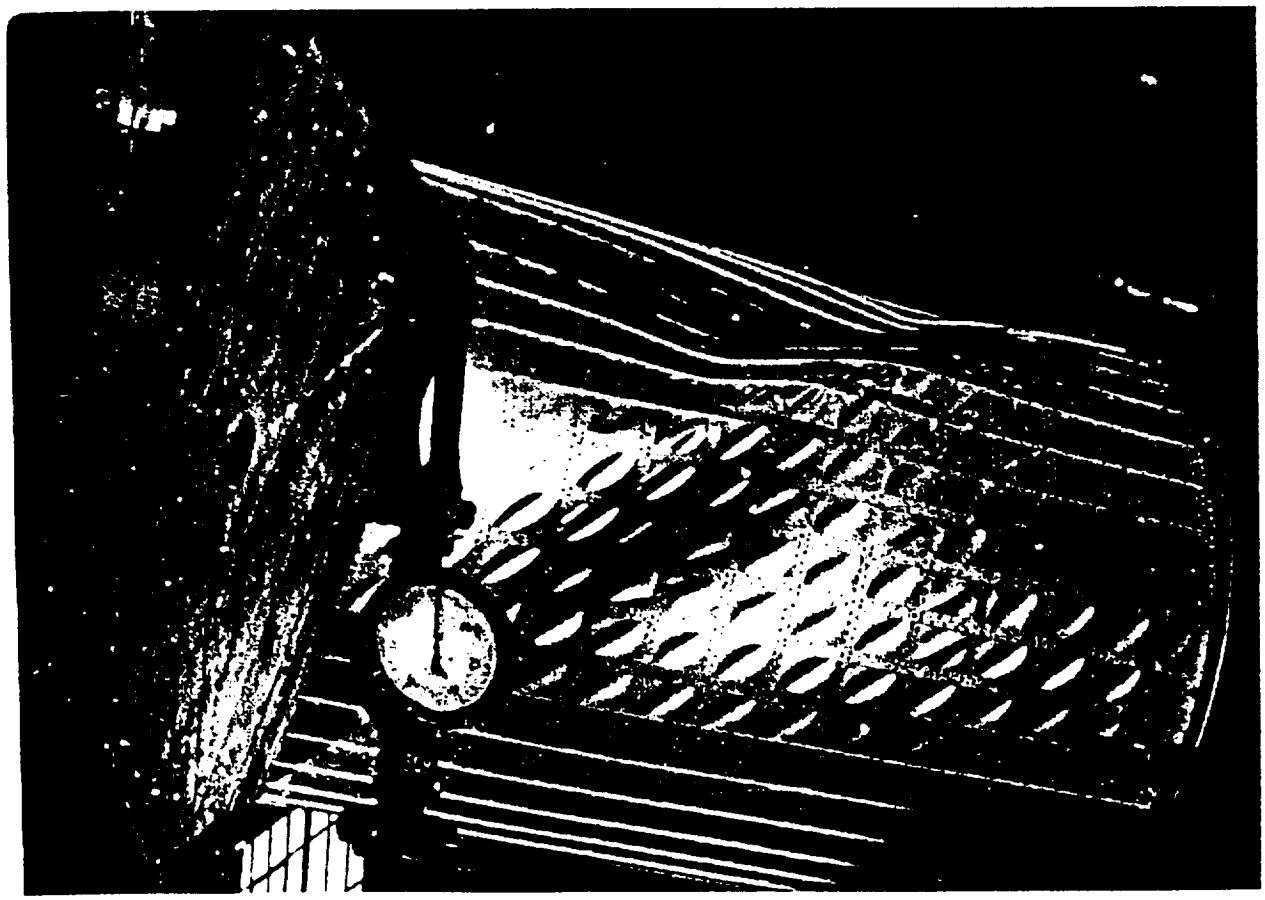

Figure 2.7. General buckling of shell

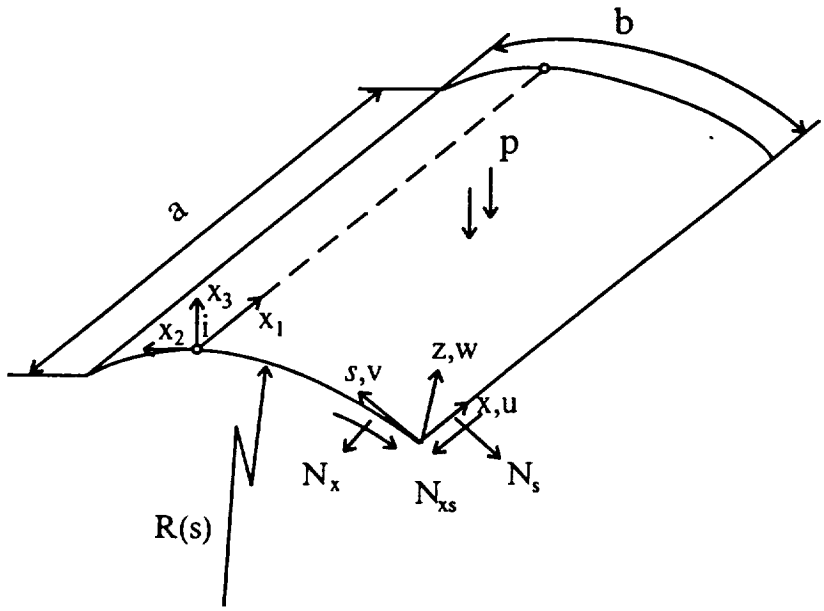

Figure 2.8. Element for evaluating anisotropic cylindrical shell

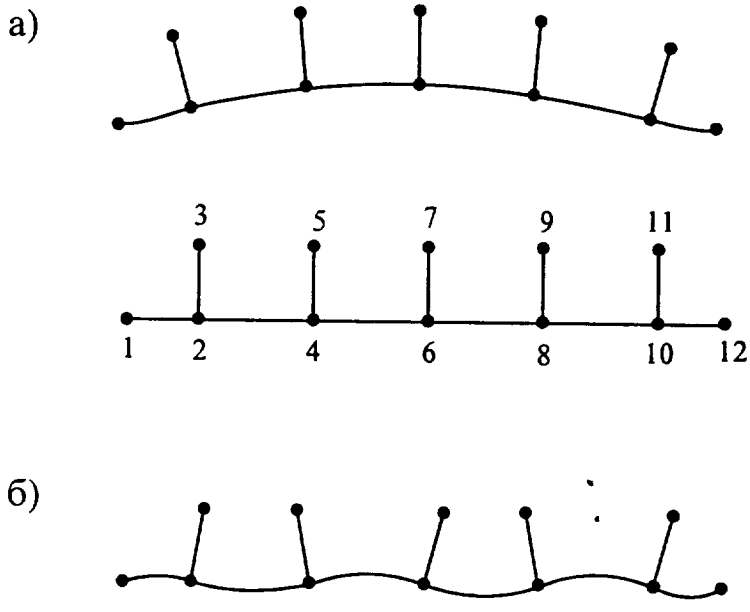

Figure 2.9. General and local panel buckling

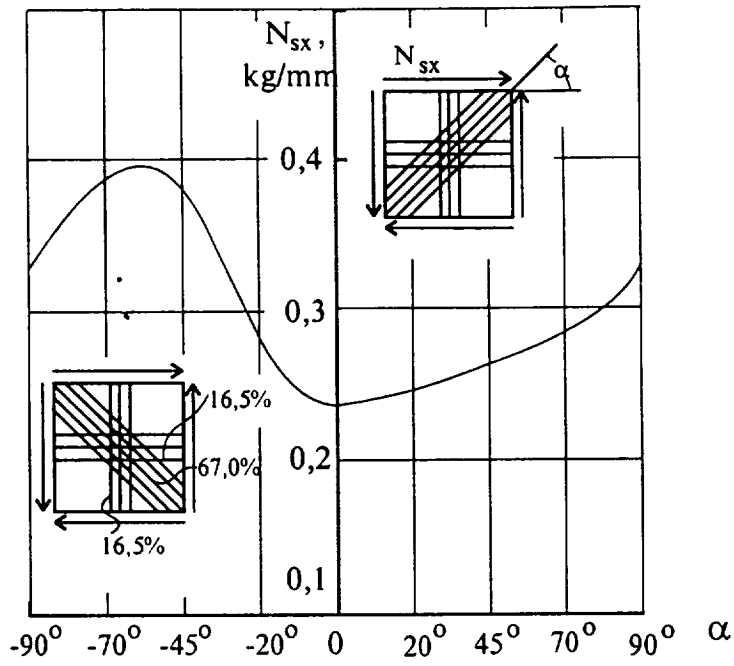

Figure 2.10. Critical shear stress resultant vs.fiber orientation angle

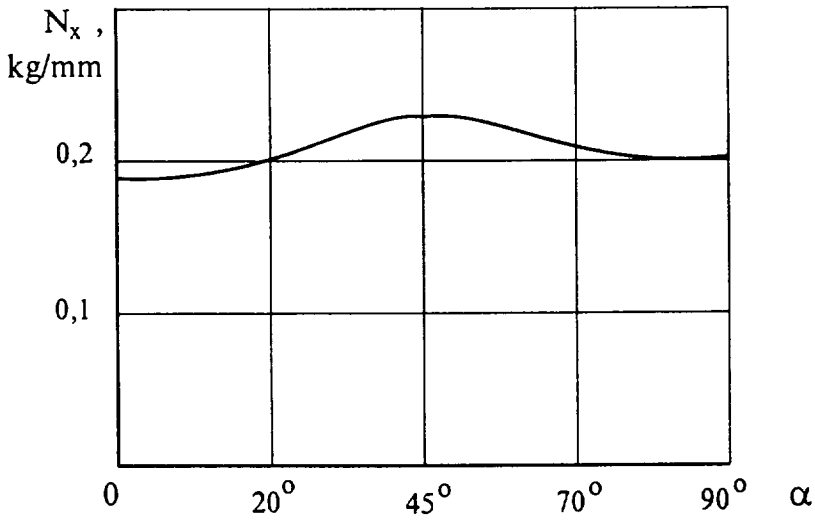

Figure 2.11. Critical compressive stress resultant as a function of the angle α

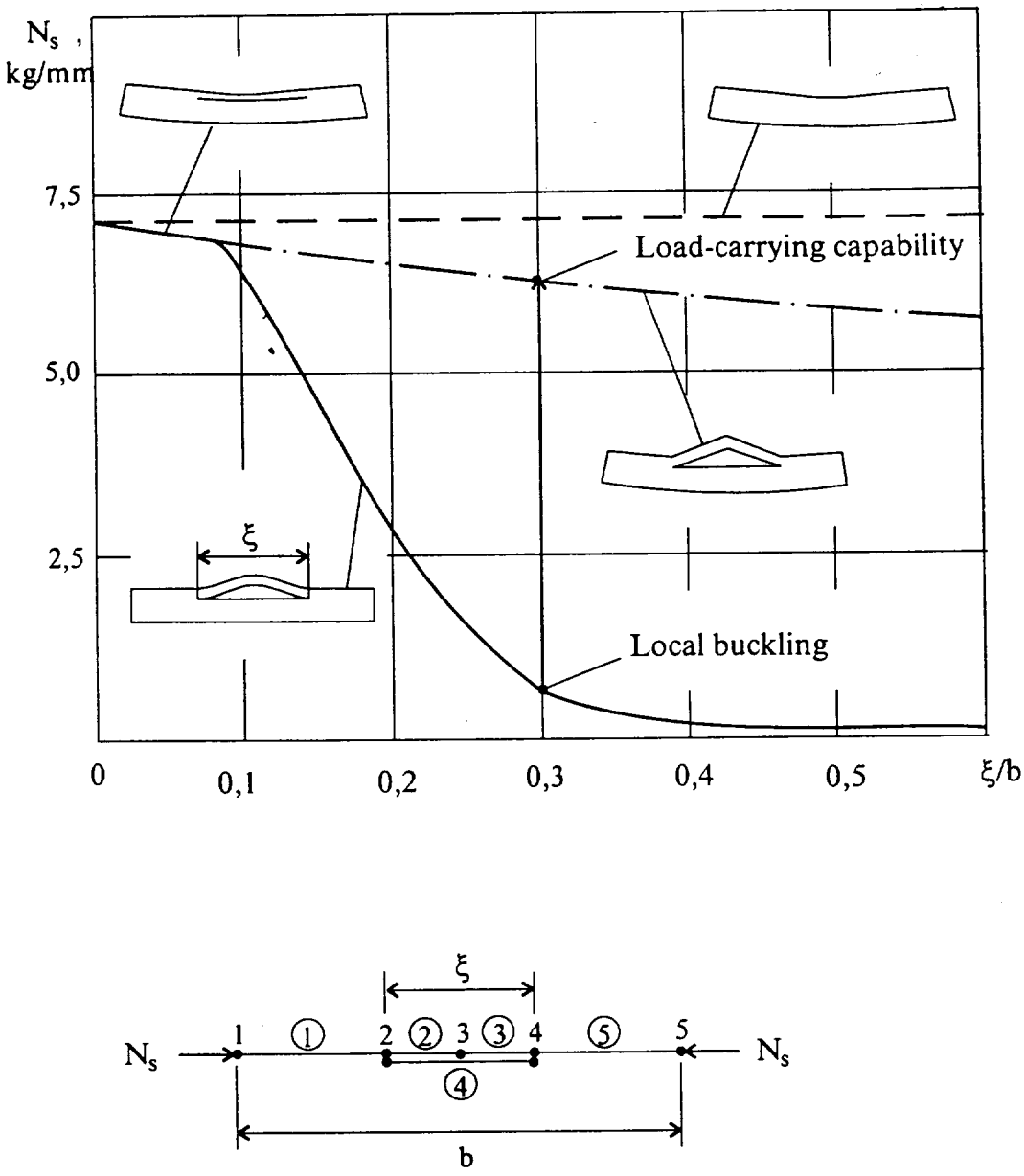

Figure 2.12. Stability and load-carrying capability of anisotropic composite plate with partial debonding